



HAL
open science

The Messinian Ebro River incision

R. Pellen, D. Aslanian, Marina Rabineau, J.P. Suc, C. Gorini, E. Leroux, C. Blanpied, C. Silenziario, S.M. Popescu, J.L. Rubino

► **To cite this version:**

R. Pellen, D. Aslanian, Marina Rabineau, J.P. Suc, C. Gorini, et al.. The Messinian Ebro River incision. *Global and Planetary Change*, 2019, 181, pp.102988. 10.1016/j.gloplacha.2019.102988 . hal-02185361v1

HAL Id: hal-02185361

<https://hal.science/hal-02185361v1>

Submitted on 5 Jan 2021 (v1), last revised 11 Sep 2020 (v2)

HAL is a multi-disciplinary open access archive for the deposit and dissemination of scientific research documents, whether they are published or not. The documents may come from teaching and research institutions in France or abroad, or from public or private research centers.

L'archive ouverte pluridisciplinaire **HAL**, est destinée au dépôt et à la diffusion de documents scientifiques de niveau recherche, publiés ou non, émanant des établissements d'enseignement et de recherche français ou étrangers, des laboratoires publics ou privés.

The Messinian Ebro River incision

Pellen, R.(1), Aslanian, D. (2), Rabineau, M. (1), Suc, J.-P. (3), Gorini, C. (3), Leroux, E. (2), Blanpied, C. (3), Silenziario, C.(4), Popescu, S.-M. (5), Rubino, J.-L. (6).

(1) CNRS, Université de Bretagne Occidentale, Univ. Bretagne Sud, UMR6538 Laboratoire Géosciences Océan, IUEM, 1 place Nicolas Copernic, 29280 Plouzané, France.

(2) IFREMER, Laboratoire Géodynamique et enregistrements Sédimentaires, BP70, 29280, Plouzané, France.

(3) Sorbonne Universités, UPMC University Paris 06, CNRS, Institut des Sciences de la Terre de Paris (iSTeP), UMR 7193, 4 place Jussieu 75005 Paris, France.

(4) Schlumberger Italiana SPA, Via dell'Unione Europea, 4 - Torre Beta, 20097 San Donato Milanese, ItalyGeoBioStratData.Consulting, 385 route du Mas Rillier, 69140 Rillieux la Pape, France

(5) TOTAL, TG/ISS, CSTTF, Avenue Laribeau, 64018 Pau Cedex, France

Keywords: NW Mediterranean Sea; Segmentation; Knickpoint; Ebro fluvial system; Messinian Salinity Crisis; Incised-valley system.

Abstract

Morphological sills condition sedimentary, water and fauna exchanges between different domains. In particular, sills are crucial factors to consider during the Messinian Salinity Crisis (MSC) palaeogeographic evolution (5.97-5.33 Ma) of the NW Mediterranean area. Here we focus on the Ebro River and its up to now unexplained short Messinian onshore length (~ 100 km) compared to that of the Messinian Rhone River (~ 480 km) despite similar present-day drainage basins. Thanks to an extensive seismic and borehole dataset, we present a new interpretation of a complete 270 km long Messinian Ebro incised-valley system course underneath the present-day continental margin and bathyal basin and its related distal detrital deposits. These results favour a syn-MSC or pre-MSC opening of the (endorheic) Ebro Basin to the Mediterranean. We propose a mechanism of retrogressive erosional process, localized at structural knickpoints that shift seaward through time. This mechanism resulted in the development of the complete incised-valley system and the falling stage system tract (FSST) during the MSC sea level fall with negligible or even null retrogressive inland erosion beyond the Catalan Coastal Range. The shifting of erosion-deposition is controlled by the pre-Messinian stepwise morphology and segmentation in the Valencia, Menorca and Liguro-Provence Basins. By comparison, the Rhone system is simpler, characterized by the key role of a single knickpoint (at the shelf-break) and a steeper continental slope. Both cases highlight the relationship between kinematic, segmentation and their relative morphologies, base-level fall and erosional/depositional response particularly well expressed during the outstanding MSC associated with a huge relative sea-level drop that we measured down to -1100m below present day sea-level.

37 **Abbreviations****General**

ESP Expended Spread Profile
Km Messinian Knickpoint
Ka Present-day knickpoint
MSC Messinian Salinity Crisis
Twt Two-Way Travel time

Geography

CCR Catalan Coastal Range
CFZ Central Fracture Zone

EB Ebro Basin
GOL Golf of Lion
LPB Liguro-Provence Basin
MB Menorca Basin
NBFZ North Balearic Fracture Zone
VB Valencia Basin

FAD First Appearance Datum
FSST Falling Stage System Tract
HST Highstand System Tract
LAD Last Appearance Datum
LST Lowstand System Tract
LU Lower Unit
MES Messinian Erosional Surface
MRS Maximum Regression Surface
MLM Messinian Lower Megasequence
MUM Messinian Upper Megasequence
MU Mobile Unit
RSME Regressive Surface of Marine Erosion
TST Transgressive System Tract
UU Upper Unit

Stratigraphy

1

2 **1. Introduction**

3 Morphological sills, whether related to sedimentary, inherited structural reliefs or originating from the
 4 kinematic history, play a crucial role in the sedimentary, water and fauna exchanges between basins through
 5 time. These sills often fit areas of different crustal nature and different subsidence histories, as observed in the
 6 Mediterranean-Paratethys area (e.g. [Leever et al., 2010](#); [Leroux et al., 2015a](#); [Palcu et al., 2017](#); [Pellen et al.,](#)
 7 [2017](#)). In the case of huge relative sea-level variations, as during the MSC (5.97-5.33 Ma) ([Manzi et al., 2013](#)),
 8 consideration of these barriers is of primary importance to understand the morphological and sedimentary
 9 evolution of the different basins (e.g. [Leever et al., 2010](#); [Flecker et al., 2015](#); [Palcu et al., 2017](#); [Suc et al., 2015](#);
 10 [Balázs et al., 2017](#)).

11 **1.1. The Ebro Paradox**

12 The Rhone and Ebro fluvial systems are excellent examples of major rivers in the Mediterranean Sea (the 2nd
 13 and 3rd respectively after the Nile) that experienced the same crisis in response to the isolation of the
 14 Mediterranean Sea. Present-day drainage areas are of similar size (nearly 99,000 km² and 86,000 km²,
 15 respectively) ([Babault et al., 2006](#)) ([Fig. 1](#)). However direct comparisons between the Messinian palaeo-Ebro
 16 and Messinian palaeo-Rhone systems point out the so-called “Ebro paradox” ([Babault et al., 2006](#)): despite
 17 similar present-day drainage areas, the length of the Messinian subaerial incision of the Ebro river seems much

18 shorter than that of the Rhone river. In the case of the Messinian palaeo-Rhone, a total 480 km long fluvial
19 incision network was described along the Alps (Clauzon, 1982, 1999) to the pre-Messinian Platform edge
20 (Bache, 2008) (Fig. 1). In the case of the Messinian palaeo-Ebro erosion system, the incision is limited to about
21 100 km from the Catalan Coastal Range (CCR) edges to the former pre-Messinian platform edge (Fig. 1)
22 (Urgeles *et al.*, 2011) with no major incision described in the endorheic Ebro Basin. Why such a difference?
23 Babault *et al.* (2006) proposed that the Ebro River did not exist before the Messinian Salinity Crisis and that
24 the connection between the endorheic Ebro Basin to the Mediterranean Sea occurred after the MSC (or
25 potentially during this phase).

26 Conversely, several authors consider that seismic data provide evidence of well-developed sedimentation and
27 deltaic progradation during the Tortonian and the development of a main incised-valley system during the
28 MSC, implying a Tortonian connection between the Ebro Basin (EB) and the Valencia Basin (VB) (e.g.
29 Cameselle *et al.*, 2014). Recent modeling and field data on the foreland EB further argued that the transition
30 from endorheic to exorheic of Ebro is pre-Messinian, although the precise timing remains to be established (12
31 to 7.5 Ma) (Fillon *et al.*, 2013; Garcia-Castellanos and Larrasoana, 2015). However, the absence of major fluvial
32 incision toward the onshore EB, the short incision of ~ 100 km and the absence of well-described detrital syn-
33 MSC deposits in the VB remain unanswered. Indeed, Messinian clastic deposits were only partially described
34 and mainly on the (present-day) outer shelf. These deposits were described either on top (Escutia and
35 Maldonado, 1992; Maillard *et al.*, 2006a,b, or below the so-called Upper Unit (UU, Garcia *et al.*, 2011;
36 Cameselle *et al.*, 2014, 2015) of the well-known Messinian trilogy (LU-MU-UU) synthesised by Lofi *et al.* (2011)
37 (Fig. 1). This peculiar morphology strongly contrasts with that of the Western, Gulf of Lion, and Eastern, Nile
38 region, Mediterranean that both show long fluvial system incisions and large detrital deposits during the
39 Messinian sea-level fall (Gorini *et al.*, 2015) and remain to be explained.

41 1.2. Geodynamic and stratigraphic framework

42
43 The Neogene palaeoenvironmental framework of the NW Mediterranean region is largely condition by
44 geodynamic history which controls the vertical motion and sedimentation in each sub-basin (Leroux *et al.*,
45 2015a, 2015b; Pellen *et al.*, 2016). The geometry and physical link between the evaporitic and detritic
46 successions, and major tectonic hinge lines are well known in the Liguro-Provence Basin (LPB, Bache *et al.*,
47 2015; Leroux *et al.*, 2015a) (Fig. 1). However, a complete regional stratigraphic and morphological seismic study
48 linking the CCR edges to the deep LPB is still lacking.

49 A NW-SE segmentation distinguishes the MB from the Mesozoic VB (Roca, 1992; Etheve *et al.*, 2016, 2018)
50 and the deep LPB (Fig 1): the Central and North Balearic Fracture Zones (CFZ and NBFZ) represent two major
51 sills that created a stepwise accommodation between the three domains (Pellen *et al.*, 2016). The geodynamic
52 process leading to the formation of these sills is rooted in the counter-clockwise rotation of Corsica-Sardinia
53 block during the early Miocene which drove the movement of Menorca Island, and non-kinematic motion of
54 Ibiza-Majorca islands (Pellen *et al.*, 2016). These motions distinguish early Miocene LPB and MB basins from
55 the Mesozoic VB basin (e.g. Olivet, 1996; Gueguen *et al.*, 1998; Bache *et al.*, 2010; Pellen *et al.*, 2016, Etheve
56 *et al.*, 2016). One of the main consequences is a different subsidence history for each basin, with purely vertical
57 Neogene “sag” subsidence for the Mesozoic VB (Pellen *et al.*, 2016).

58 A NW-SE segmentation shapes the GOL-LPB with five differentiated crustal domains on the French side
59 (Moulin *et al.*, 2015; Afilhado *et al.*, 2015; Jolivet *et al.*, 2015): unthinned continental crust, thinned
60 continental crust, highly thinned continental crust, exhumed lower continental crust and proto-oceanic crust.
61 Three domains of subsidence were found defined by three hinge lines (Fig.1, 2). On the platform and slope,
62 the subsidence takes the form of a seaward tilt with different amplitudes, whereas the deep basin (with exhumed
63 lower continental crust and proto-oceanic crust) subsides purely vertically (Leroux *et al.*, 2015).

64 The shelves of the MB and the GOL (domain 2a) (Fig. 1) first record a late Oligocene-Aquitania marine influx
65 (Roca and Guimera, 1992; Roca *et al.*, 2001; Bache *et al.*, 2010), followed by Burdigalian-Tortonian clay-marl
66 then sand deposits associated with a prograding trend. The outermost position of this Tortonian shelf is shown
67 on Figure 1 (from Bache, 2008). The deep part of the LPB and MB are usually associated with condensed
68 Burdigalian-Tortonian deposits (Roca *et al.*, 2001). The Mesozoic VB (Roca, 1992; Etheve *et al.*, 2016, 2018)
69 experienced the first marine ingression during the late Burdigalian-Langhian followed by an enhanced
70 Tortonian prograding trend in the Tortosa area (Clavell and Berastegui, 1992; Cameselle *et al.*, 2014; Pellen *et al.*,
71 *et al.*, 2016).

72

73 1.3. Ebro versus Rhone inheritances

74 The initiation of the endorheic sedimentation in the EB has been estimated at ~35 Ma (Costa *et al.*, 2010),
75 the final preserved lacustrine fill -stage is proposed to be at least 13.5 and 12 Ma (in Urgeles *et al.*, 2011) and
76 up to Tortonian (e.g. Vasquez-Urbez *et al.*, 2013). At the time of the basin’s opening towards the Mediterranean
77 Sea, an elevation of 535-750 m above sea level has been estimated (Garcia-Castellanos and Larrasoña, 2015)
78 which places the Catalan Coastal Range (CCR) as an important morphological barrier between the VB and
79 EB. At the dawn of the MSC, a stepped morphology is observed for the VB-MB where offshore knickpoints

are located at the edge of the Miocene platform or at major geodynamic boundaries (Fig. 2). On the contrary, the GOL is characterized by a single continental slope (Guennoc *et al.*, 2000). Furthermore, no major geodynamical sill is observed along the onshore Rhone drainage system (Séranne, 1999; Guennoc *et al.*, 2000; Sissingh, 2001).

In this study, based on a large set of seismic and borehole data, we made a detailed synthesis of the offshore physiography during Messinian, by correlating the VB, MB, and LPB with seismic stratigraphic and geomorphological methods tied to existing borehole data with revisited detailed biostratigraphic analysis to propose a new understanding of Ebro and Rhone systems evolution during the MSC.

2. Data and Method

2.1. Dataset

Our study is based on a large set of seismic and borehole data collected during the extensive French academia-industry programs (Actions-Marges, GRI Tethys Sud), in close collaboration with the Total and Schlumberger groups as well as data available from the Spanish SIGEOF database. This compilation provided for the correlation of seismic markers from the VB towards the LPB (as shown already in Pellen *et al.*, 2016). Twenty-four petroleum wells drilled between 1969 and 2004 along the NE Iberian margin have been used to calibrate seismic interpretations, although the stratigraphic information was often sparse or vague. We used the detailed stratigraphic, sedimentological and micropaleontological information available from three wells located on the present-day Ebro platform to constrain ages and palaeoenvironments of identified surfaces and units: Fornax 1 (Bailey *et al.*, 2008; Urgeles *et al.*, 2011; Cameselle *et al.*, 2014; Mauffrey *et al.*, 2017), Benicarlo C1 (this study) and Tarragona E2 (Evans *et al.*, 1978 ; Bessais & Cravatte, 1988).

In this paper the detailed lithological, environmental and biostratigraphic information from the Benicarlo C1 are provided for Miocene-Messinian-Pliocene series (based on Evans *et al.*, 1978) that we have revisited in the light of recent biostratigraphic charts, a modern geological time scale (Gradstein *et al.*, 2012) and correlation with more regional information (see chapters 3.2 to 4.2).

2.2. Sequence stratigraphy

Conventional seismic stratigraphic method was used (Mitchum & Vail, 1977; Vail *et al.*, 1977) to identify seismic discontinuities and stratigraphic surfaces and units based on reflexion configurations and facies characteristics (See the Table in Supplementary Material 3 for details of surfaces and units). However, identified surfaces and units were interpreted using principles of sequence stratigraphy in their revised most recent

112 version i.e. including interpretation of Falling Stage System Tract (FSST) (e.g. [Hunt and Tucker, 1992](#);
113 [Catuneanu et al., 2011](#)), forced regression concept (e.g. [Plint et al., 1988](#)) with Maximum Regression surface
114 (MRS) and Regressive Surface of Marine erosion (RSME) (e.g. [Helland-Hansen and Hampton, 2009](#)). Ages of
115 these sequences were provided by well data. Our interpretations were then integrated into the 'Kingdom Suite'
116 software to insure coherency at all crossing lines. For the Messinian units, we used the now well established so-
117 called « Messinian-trilogy » Lower Unit (LU)/Mobile Unit (MU)/ Upper Unit (UU) as synthesized by [Lofi et al.](#)
118 ([2011](#)). Nevertheless, we provide special focus on units and sub-units related to clastic units (see results below).

121 2.3. Time to depth conversion and backstripping

122 Our seismic interpretations were converted from time to depth using average sediments velocities (layer cake
123 model), to obtain the geometries in depths (meters) of surfaces and sedimentary units ([Fig. 3, Transect01](#)).
124 Seismic velocities strongly vary in space within the same stratigraphic interval, with significant variations
125 between the shelf, the base of slope, and the basin. Compiled borehole velocities on the VB platform and on
126 the foot slope, as well as ESP velocities located in the deep LPB ([Leroux et al., 2016](#)) were used to estimate an
127 average velocity for each layer (see velocity model in [suppl. mat. 1](#)). The depth converted profile allowed us to
128 measure the difference in altitudes between key points along the profiles, and sedimentary unit thicknesses.
129 A simple 2-D backstripping was performed to reconstruct geometries through time (in particular at early
130 Zanclean, at Messinian low stand incised-system and related deposits (see details in [suppl. mat. 2](#)). Input
131 parameters for the VB domain include paleobathymetry, age, and porosity of sedimentary packages based on
132 [Urgeles et al. \(2011\)](#). An estimated total subsidence value up to 960 m/Ma for the deep LPB domain was also
133 applied to the 2-D backstripping for Pliocene-Quaternary times as quantified by [Rabineau et al., \(2014\)](#).

135 2.4. Knickpoint definition and chosen approach

136 Our study used the identification of knickpoints, highlighted either by morphological change or new
137 sedimentary sequences development along the seismic profile. Different processes are associated with onshore
138 and offshore development of such morphological features. On land, knickpoints are interpreted as resulting
139 from renewed erosion of a rejuvenated river that propagates upstream and influences the development of
140 landscapes and source-to-sink systems ([Grimaud et al., 2016](#)). They are usually triggered by a relative fall in river
141 base-level (either through eustatic sea-level drop, tectonic faulting or uplift) and can also highlight the onshore-
142 offshore position ([Goswani et al., 2016](#)). Submarine knickpoints are often located at the shelf-break creating

143 an offlap-break either (i) at the transition between the outer shelf and the continental slope (e.g. Rabineau *et*
144 *al.*, 2014), or (ii) at the boundary of domains where tectonic motion displaces the seafloor (Amblas *et al.*, 2011)
145 or (iii) at the site where channel levees are breached. Knickpoints are key elements to take into account in
146 when considering segmented domains, we therefore paid a particular attention to their identification.

147 Below, we present our results from the onshore domain towards the deeper offshore domains.

149 3. Results

150 3.1. Morphology from seismic interpretation

151 **Figure 3** presents our stratigraphic interpretation across the VB-MB along six seismic profiles perpendicular to
152 the main erosional incision. Transect 01 has been converted to depth. Eight major seismic surfaces are
153 illustrated, S0 (Tertiary basement), MES, S11, S20, S21, S22, S24, and S30 which respectively delimit four
154 seismic units: SU12a-c, LU, MU and UU and three major knickpoints (Km1-3). Three secondary surfaces
155 (S26a, b, c) are also identified in the UU. Relationships, age and interpretations of surfaces and units are
156 presented in the table in [suppl. mat. 3](#).

157 The first knickpoint Km₁ is located at the transition between the former foreland EB (~ 535 m above sea level)
158 and the VB at the edges of the CCR (**Figs. 2 and 3**). Below this knickpoint, the Marginal Erosional Surface
159 (MES, Lofi *et al.*, 2011) shows a highly rugged and dissected surface with frequent incisions organized in a
160 dendritic pattern (also interpreted on 3D seismic data, e.g. Urgeles *et al.*, 2011, and Comeselle *et al.*, 2014)
161 (**Figs. 2 and 3, section a**). Four palaeo-drainage systems are observed (**Fig. 2**) that present numerous incised
162 fluvial tributaries with rough badland-like morphology of the MES (Urgeles *et al.*, 2011) above the isocontour
163 of 1.6 sec TWT (~ 2.5 km depth) below present-day sea level. It is worth noting that the MES truncates the
164 former Tortonian prograding clinoforms which form the Miocene platform in the Tortosa-Ebro domain (**Figs.**
165 **3 and 4**). This is also confirmed by the Tarragona E2 well which sampled Tortonian deposits just below the
166 MES (Bessais & Cravatte, 1988). A wide dendritic palaeo-drainage system is mapped for the Tortosa-Ebro
167 domain (**Fig. 2**) which is the main and deepest NW-SE river channel interpreted as the Messinian Ebro fluvial
168 system (Urgeles *et al.*, 2011) (**Fig. 2, 3 section a & b**). A ~ 61 km long main channel incision can be measured
169 from the pre-MSC coast to the Tortosa-Ebro lower slope.

170 The erosive surface S11 extends seaward of the MES at the position of the Km₂ (**Fig. 3, Transect01 - km 130;**
171 **Fig. 4**) at the Miocene platform edge, delimiting the base of SU12a showing downlapping prograding
172 clinoforms geometries. Only the bottomset part of the clinoforms has been preserved on both sides of the main
173 Messinian river channel. The basal erosive surface S11 also marks a change in the progradational trend along

174 the Miocene platform edge (Fig.4, section h) of the Tarragona area: A major change in direction of sediment
175 input from the morphological domain of Barcelona to the Tortosa-Ebro domain is highlighted by the basal
176 erosive surface S11.

177 S11 shows a generally smoother morphology towards the VB foot-slope domain. In this area the MES subtracts
178 into two erosive surface: the basal erosive surface S20 which truncate the seismic unit SU12a while the top
179 erosive surface S30 bound the UU seismic unit (Fig. 3, sections c, d). Along the former Miocene outer shelf,
180 the MES-S20 surface shows a smoother erosive surface below 2.5 km depth (Fig. 4, sections g, h) with the
181 disappearance of badland morphology except in the axis of the main channel incision (Fig. 3, section b; Fig.
182 4). The extension of the S20 surface across the VB foot-slope domain highlights the lateral continuation of an
183 incised channel along the VB domain. A slight NE-ward inclination is observed along the incised-valley profile
184 with a mean present-day depth position ranging from 2.8 km below sea level at the Tortosa domain foot-slope
185 to 3.2 km depth at its outlet (Fig. 3, sections c-f). The morphology shows an evolution from a ~6 km wide with
186 an interfluvial/thalweg height of 370-400 m at the toe of the proto-Ebro slope offshore the Tortosa-Tarragona
187 domain (Fig. 3, sections a-c) to a ~16 km wide, 100-130 m deep incision at the transition towards the MB (Fig.
188 3, sections d, e). Bedrock morphology partly deflects the path of the incised-valley and slightly influences its
189 sinuosity (Fig.2; Fig. 3, section c).

190 On both sides of this SW-NE valley, which totals a length of ~134 km in the deep VB domain, the surface is
191 relatively conformable compared to the underlying deposits. The main incised-valley is joined by two smaller
192 tributaries from the SW part of the VB and already mapped by Comes et al. (2015).

193 At the transition between the VB and MB (CFZ area in Figs. 2, 3 and 5, section i) (Maillard and Mauffret,
194 1999; Pellen et al., 2016), S20 shows another knickpoint Km₃ (~3.2 km depth, at Transect01, km 270 in Fig.
195 3). It marks: 1) the deepening of the basal surface S11 and its overlying unit SU12c – as the lateral correlation
196 of SU12a; 2) the last S20 toplap features; 3) the formation of two new surfaces, S21 – as the lateral correlation
197 of S20 – and S22 at the top and 4) the thickening of the UU.

198 The S12 and S21 surfaces delimitates the development of SU12c with the NE-ward preserved prograding
199 clinofolds (Fig. 5, section j). S21 at the top of SU12c also shows some widespread erosion and becomes
200 smoother and conformable towards the MB-LPB transition (Fig. 3, section f). The conformable and non-incised
201 S21 development also highlights the formation of the overlying LU. Both observations attest the termination
202 of the trans-VB incised-system thus marking its outlet at the VB-MB transition.

203 The continuity of the erosional system from the VB platform to the Km₃ knickpoint therefore points to a 270
204 km long system that we identify as the trans-VB Messinian valley system (Figs. 2 and 3, Transect 01 and sections
205 b-d). The MB-LPB transition marked by the North Balearic Fracture Zone (NBFZ) corresponds to the full

206 development of the Messinian trilogy units (LU-MU-UU) as identified in the deep LPB domain (Figs. 3 and
207 9).

208 Using the backstripped section of Transect01 at 5.3 Ma (i.e. at the end of the MSC), we measure the general
209 slope of the MES-S20-S21 from 90 to 430 km as equal to 0.55 % (i.e 0.32 °). However, individual segments in
210 between knickpoints show a slope even smaller than 0.4 % (0.23°) and 0.45% (0.26°), between 90-280 km and
211 310-430 km respectively. Conversely, surface S11 at the base of SU12c shows a slope of 1.58% (0.9 °), between
212 310 and 430 km.

213 214 215 **3.2. Borehole data**

216 **3.2.1. Biostratigraphy**

217 The Benicarlo C1 well (Fig. 6) provided planktonic foraminifers recorded from cuttings (Evans *et al.*, 1978).
218 These data have been re-visited and evaluated in light of the most recent biostratigraphic zonation in the
219 Mediterranean (Iaccarino *et al.*, 2007) and the modern geological time scale (Gradstein *et al.*, 2012).

220 The top of Cretaceous limestones (Upper-Middle Cenomanian) is well identified at 4330 m depth. With
221 respect to several Mediterranean long records (Suc *et al.*, 1992; Lirer and Iaccarino, 2011), the base of
222 Pleistocene deposits (i.e. the base of the Gelasian, at 2.6 Ma) can be assessed between 2330 m depth (uppermost
223 occurrence of *Sphaeroidinellopsis subdehiscens*, usually estimated at 3.2 Ma) and 2060 m (lowermost occurrence
224 of *Globorotalia inflata*, dated at 2.09 Ma in the Mediterranean Sea; Iaccarino *et al.*, 2007). Consequently, our
225 biostratigraphic re-evaluation focuses on the depth interval 4300–2300 m, which encompasses the Middle-Late
226 Miocene and whole Pliocene (Fig. 6). Examining the vertical distribution of the species with a biostratigraphic
227 significance along the studied interval, we paid particular attention to discontinuous occurrences, some
228 punctual records may result from cavings or reworkings.

229 *Orbulina universa* is present from 4240 m depth that suggests an age younger than 14.10 Ma (First Appearance
230 Datum, FAD, of the species in the Mediterranean; Iaccarino *et al.*, 2007). *Neogloboquadrina acostaensis* has been
231 continuously recorded from 4240 to 4180 m, then intermittently at 3830 m, and continuously from 3710 m
232 to 2040 m. The FAD of *N. acostaensis* in the Mediterranean Sea is dated at 11.90 Ma. Two interpretations can
233 be discussed: (1) to place the FAD of *N. acostaensis* at 4240 m or (2) to place it at 3710 m. Hypothesis 1 implies
234 very thick deposits to be ascribed to Tortonian while hypothesis 2 suggests that deposits from the base of the
235 studied interval partly belong to the Serravallian and maybe to the Langhian. Caliper log (Fig. 6) suggests the
236 presence of numerous caving effect between 3600 m and 4240 m which would affect the record of *N. acostaensis*
237 or *Orbulina universa* below 3710 m. As well, the biostratigraphic interpretation of the nearby Tarragona E2 well

(Cravatte, 1980; Bessais, 1984; Bessais & Cravatte, 1988) would be more consistent with the second hypothesis. Accordingly, sediments between 4240 and 3710 m depth could belong to a time-interval running from biozone MMi5 to biozone MMi10 (Fig. 6).

Above, the continuous occurrence of *Neogloboquadrina humerosa* is recorded from 3230 m. The FAD of *N. humerosa* is placed within biozone MMi12 (Iaccarino *et al.*, 2007), in agreement with the identification of this biozone in the Benicarlo C1 well (Fig. 6). A similar comment can be expressed for *Globigerinoides extremus*, which has been continuously recorded in the Benicarlo C1 well between 3220 m and 2900 m, that is also conceivable with the FAD of the species at the base of biozone MMi12 (Iaccarino *et al.*, 2007).

The occurrence of *Globorotalia conomiozea* from 3110 to 2640 m characterizes the MMi13 biozone ending at 5.97 Ma (Iaccarino *et al.*, 2007). Then, *Globorotalia margaritae* and *Spheroidinellopsis paenedehiscens* are recorded together from 2535 m, indicating the biozones MPI1-MPI2 up to the first record of *Globorotalia puncticalata* at 2511 m indicating the base of biozone MPI3 (Iaccarino *et al.*, 2007). Finally, the uppermost record of *Globorotalia margaritae* at 2370 m is used to delimit the top of biozone MPI3, dated at 3.80 Ma. These data are transferred to Fig. 6 where the ages of the biozone boundaries are also indicated according to Iaccarino *et al.* (2007). It is thus obvious that an important portion of the deposits drilled at Benicarlo C1, more precisely those between 3110 m and 2511 m depth, belongs to the pre-evaporitic phase of the Messinian.

3.2.2. Lithologies and Environments

The very thick sequence of volcanic tuffs and lavas between 4315 m - 3730 m were deposited in a fairly shallow marine environment during late Serravallian-Early Tortonian time as shown by the thin interbeds of soft limestones containing rare *Amphistegina* sp. and planktonic foraminifera (Evans *et al.*, 1978).

The sequence between 3695-3016 m, of Tortonian age is of open marine, outer sublittoral to bathyal nature. The onset of colder water conditions over this interval is shown by the presence of sinistral coiled specimens of *Globorotalia acostaensis* (since around 3400m) before the warmer Messinian period (Suc *et al.*, 1995; Evans *et al.*, 1978).

The interval 2810-2525 m represents a shallowing upward phase, with the probable formation of underwater supra-littoral conditions at the top. The reduction in planktonic foraminifera and the upward coarsening of the sediments suggests a general shallowing of the basin at this time.

The interval between 2525 - 2500 m can be separated in two parts: the topmost part of this interval between approximately 2510 - 2500 m as well as interval 2525 - 2524 m contain thin beds of white algal limestone interbedded with white sandstone and yellow to ochre marl/claystone. The lower limestone contains anhydrite.

270 Additionally, the occurrence of a single cyprid ostracod, algae and bryozoan in the 2515 and 2525-2520 m
271 ditch cuttings sample is taken to indicate both a stratigraphic and environmental break at this level and possibly
272 reflects the establishment of brakisch - non-marine conditions (Evans *et al.*, 1978).

273 The interval 2500 - 2370 m is characterized by soft, light grey calcareous shales and marls/claystone with minor
274 sand stringers throughout. This interval is assigned to the Ebro Group, Early Pliocene, deposited in an open
275 marine environment.

276

277

278 4. Discussion

279 4.1. Age assignment and sequence stratigraphy interpretation

280 Combining the results from seismic interpretation in correlation with biostratigraphy from Benicarlo C1 well,
281 we consider that the Messinian is represented mostly by marine sediments from 3016 to 2525 m depths, i.e.
282 491 m in thickness with a shallowing upward trend (Fig. 6). The proximal to distal correlation of seismic units
283 SU12a to SU12c (both topped by the MES-S20) also shows a downward-shift of uppermost surface (as seen on
284 depth-converted seismic transect shown in Fig. 3 and in backstripped section (Supp. Material 2).

285 The MES(-S20) is depicted as the maximum regressive surface (MRS in the sense of Catuneanu *et al.*, 2011)
286 and is located at 2525 m in the Benicarlo C1 well. This MRS (MES) would be dated at 5.6 Ma according to
287 Clauzon *et al.* (1996, 2015) and CIESM (2008). The underlying Messinian sediments (SU12a and SU12c)
288 therefore correspond to the remaining sediments of the Falling Stage System Tract (FSST). According to our
289 seismic interpretation, the erosive surface at the base (S11) may correspond to the regressive surface of marine
290 erosion during the falling stage of the MSC crisis, also described in Quaternary sequences related to 100 000
291 years cycles (Rabineau *et al.*, 2005). However, some early pre-MSC Messinian sediments seem to be preserved
292 as biostratigraphic data suggest with the presence of *Globorotalia Cibaoensis* around 3000 m but considering the
293 relative Messinian sea level fall velocity and amplitude, earlier pre-MSC deposits are very fortunate to be
294 reworked and preserved in MSC related deposits.

295 This interpretation of the FSST for SU12a is supported by the fact that Benicalo C1- shows sediments of a
296 younger age than those found in both Fornax-1 and Tarragona E2 wells (Evans *et al.*, 1978 ; Bessais & Cravatte,
297 1988; Urgeles *et al.*, 2011) as well as a progressive downward shift of MES-S20 surface. Our seismic
298 interpretation and correlation suggest that SU12c is also part of this FSST and in fact represent the end of it
299 with the most distal regressive deposits. Development of SU12c unit is followed by the initiation of the LU as

300 lowstand system tract (in the sense of [Boyd et al., 2006](#); [Gorini et al., 2015](#)) (Fig. 8, stage 3). This FSST and
301 LST would correspond to the MLM (Messinian Lower Megasequence) of [Gorini et al. \(2015\)](#).
302

303 Unfortunately, no well exists to sample this unit SU12c, so we have no direct related biostratigraphic
304 information, which could confirm or invalidate this hypothesis.

305 Above the MES at Benicarlo C1, the occurrence of a single cyprid ostracod, algae and brozoan in the 2515 m
306 and 2525-2520 m cuttings suggest that this thin unit going from probable emersion to shallow water
307 environments records the end of the MSC. Following [CIESM \(2008\)](#) or [Bache et al., \(2012\)](#) scenarios, this unit
308 could be interpreted as corresponding to those deposited during the early marine reflooding of the
309 Mediterranean Basin (Transgressive System Tract) that preceded the base of the Zanclean, and estimated
310 between 5.46 - 5.33 Ma. This TST is overlain by a clear open-marine high stand System Tract (HST) with warm
311 conditions in early Zanclean Pliocene. (5.33-3.85 Ma) ([Suc et al., 1995](#)).
312

313 **4.2. Subaerial versus submarine erosion and position of the Messinian shoreline**

314 Erosional surfaces may develop in subaerial or submarine environments. However, process and formation
315 of erosional surfaces differ in the air and under water, due to the varying physics of the different fluids. In
316 subaerial environments topography is highly variable. Landscapes are carved by rivers and strongly dependent
317 on precipitation that will erode and transport sediment as a function of gravity and slopes as the primary
318 controls. In submarine environments, widespread erosion also occurs: both in proximal environments (at the
319 shoreline and on the shelf) with a strong impact of waves, tides and currents but also in deep environments
320 such as submarine canyons, slopes and deep-sea areas with processes such as turbidity currents, landslides,
321 debris flows (e.g. [Amblas et al., 2006](#)) and contour currents (e.g. [Rebesco et al., 2014](#)). In shallow environments
322 (between 0 to 100 - 150m) a very efficient erosion process is related to wave action. The main result of this
323 wave action is the creation of large smooth morphologies and wave-cut terraces that are recognized worldwide
324 throughout the geological time scale (e.g. [Cattaneo and Steel, 2003](#); [Catuneanu 2006](#); [Bache et al., 2014](#)).

325 In our case study, S11 marks the first MSC regressive surface of marine erosion (RSME) prior to the MES
326 development (see also above) and highlights Km₂ at an onshore-offshore position ([Goswami et al., 2017](#)). The
327 overlying U12a clinofolds (VB area) correspond to the Messinian forced-regressive prisms (FSST), with erosion
328 and redeposition of sediments in the forced-regressive prisms ([Fig. 4, section g](#); [Fig. 6](#)) and a MRS at the top.
329 The subaerial development of the Trans-VB incised-valley system is attested across the Tortosa-Ebro domain
330 with rugged badland-type morphology, terraces, fluvial meanders, oxidation surfaces (Fornax-1) as fully
331 explained in ([Urgeles et al., 2011](#); [Cameselle et al., 2014](#)).

332 Moreover, as shown is the results section: the general slope of backstripped MES-S20-S21 erosional
333 surface is only 0.55% (0.32°) or even less in segments between knickpoints (0.23° to 0.26 °). These slope
334 gradients are much smaller than any present-day well-defined submarine canyon. In the GOL, the shelf-break
335 occurs when slope gradients reach 1%. Gradients < 1% delimit the continental shelf, whereas gradients > 1%
336 correspond to the upper slope. The values obtained for the Messinian MES-S20-S21 are typical of low shelf
337 gradients and not slope gradients where submarine canyons occur, they are generally between 2 and 5 ° in
338 canyon head areas in the GOL (Baztan *et al.*, 2005). Another example is provided by present-day submarine
339 canyons in the VB that all show slopes around 10° in upper slope submarine canyons to 2-4° at the base of
340 slope canyons (Amblas *et al.*, 2006). Those values are more than one order of magnitude higher than what we
341 measured here. MES-S20 general shape cannot be related to any submarine canyon mechanism.
342 If MES-S20 might have been also initiated as submarine one, this composite erosive surface was then re-worked
343 as a subaerial surface of erosion related to the Messinian lowermost sea level (MRS) with a coastline that
344 reached at least km₃ (270 km; Fig. 3 Transect 01). Its outlet is associated with the development of SU12c after
345 the Km₃ knickpoint and the start of S11c erosional surface at its base. The limit of prograding SU12c unit
346 would thus correspond to the most distal detritic products related to the relative MSC sea level fall stage.

347
348 The Messinian shoreline (Fig. 3 Transect01; Fig. 5, section I and Supp. Mat 2) existed at least up to km 270.
349 In any event, the minimum lowest MSC sea level (at km₃) was around -1100 m below present day sea-level
350 according to the backstripped section, SU12c corresponds to the final development of the detritic product
351 related to the MSC sea-level fall. The values we give here for sea-level reconstruction are probably maximum
352 values as backstripping was conducted up to 5.3 Ma after the UU deposition (and not 5.6 Ma at the maximum
353 sea level drawdown).

354 355 **4.3. A model for the Messinian Ebro incised-valley formation: Segmentation, knickpoint role, and** 356 **palaeogeographic implications.**

357
358 The model in Fig. 7 attempts to explain the Ebro paradox and the following scenario, which highlights the
359 multiple versus single knickpoint model implication in the fluvial dynamic during relative sea-level change.
360 From this simplified model, identification of a 270 km long Messinian Ebro incised-valley system and its
361 infilling by detrital FSST deposits allows us to propose an explanation clarifying the relationship between
362 drainage areas and the Messinian fluvial incision.

363 The existence of a pre-Messinian physiography and segmentation in the Valencia Basin (Pellen *et al.*, 2016)
364 plays a crucial role in its subsidence history, with an induced pre-Messinian step-by-step seafloor deepening
365 between the sagged VB, the MB and the deep LPB (Figs. 7 & 8a, stage 1).

366 Prior to the MSC sea level fall, the gradual restriction of the marine connections (CIESM, 2008; Roveri *et al.*,
367 2014) would imply relative minor sea level variation. As a fact a first retrogressive erosion Km_1 is located at the
368 CCR area, following the principle of the river equilibrium profile (Miall, 2013). The result is the initiation of
369 S11 basal erosive surface at the platform edge (Km_2) (Fig. 8a, Stage 1) and the detrital sediment deposition
370 (SU12a) offshore fluvial systems.

371 The progressive limitation of exchanges followed by the abrupt break of water exchanges through the Rifian
372 strait (Krijgsman *et al.*, 1999) at 5.60 Ma resulted in a rapid sea-level fall within the Mediterranean Basin. The
373 sea level quickly reached Km_2 (Fig. 8a, Stage 2a) implying a shift to the outermost limit of the Miocene platform
374 of the main retrogressive erosion. The eroded products were gradually deposited along the former Miocene
375 slope area, forming the SU12a unit (as drilled in Benicarlo well and showing ages of at least 6.14 to 5.72 Ma).
376 With the sea-level fall continuing, up to 5.6 - 5.45 Ma depending on the chronostratigraphy of the discussed
377 scenarios (i.e. CIESM, 2008; Bache *et al.*, 2012, 2015; Gorini *et al.*, 2015), the main regressive erosion shifted
378 again and the upper part of S12a was partially reworked and redeposited in the offshore domain as in FSST or
379 Forced regression models (Gorini *et al.*, 2015). Little detrital SU12a formation is observed at the VB base of
380 slope because, between stage 2a and 2b (Fig. 8a), the accommodation space in the Valencia foot slope area was
381 too small to accumulate thick series. This implies intense sedimentary transfer from the subaerial eroded
382 platform domain directly to the deep marine Menorca and Provence domains. When the sea level reached
383 Km_3 , the fluvial base-level and main retrogressive erosion migrated to the Valencia-Menorca transition with
384 clear erosional truncations (Fig. 8a, stage 2b) and the detrital sedimentation was transferred to the Menorca
385 and Provence deep domain, as shown by the development of the SU12c prograding clinoforms. At the lowest
386 sea-level, our interpretations locate the shoreline at Km_3 , observed on the CFZ axis (Fig. 3).

387 This evolution of downward shift erosion and the clear shift of the depocentres towards the deep basin
388 is typical of a falling stage system tract that occurs on rather flat areas separated by steps which involve a
389 proximal regressive erosion together with a distal retrogressive erosion at the step (knickpoint). As the sea-level
390 fall continues, we observe a quick shift of this double erosion from Km_1 to Km_3 . With this mechanism, the
391 river equilibrium profile has to be well developed at Km_3 so as to observe major retrogressive erosional process
392 at Km_2 area. Depending of the inertia of the retrogressive erosion dynamics at each knickpoint, there is no
393 increased fluvial erosion nor propagation towards the onshore Ebro areas as in the case of the Rhône (see

394 below). The existence of the CCR may also further prevent the propagation of the fluvial erosion towards the
395 inner parts of the EB.

396 In the Rhone system, earlier work showed the existence of three hinge lines in between different
397 structural domains related to the opening of the LPB. The model in Fig. 8b (stage 1-4) illustrates the
398 development of Messinian Pyrenean-Languedocian and Rhone fluvial systems during the MSC sea-level drop,
399 based on the work of Bache *et al.* (2009, 2010, 2012, 2015) and Gorini *et al.* (2015). Domain 2b corresponds
400 to the main geodynamic sill which records the gradual transition between marine and aerial domain during
401 the MSC sea-level fall (5.6-5.55 Ma) i.e. Gorini *et al.*, 2015) and slow sea-level rise (formation of wave
402 ravinement erosion surface between 5.55-5.46 Ma if we follow Bache *et al.*, 2012 scenario). Only minor onshore
403 knickpoints are mapped along the Rhone fluvial profile (Clauzon, 1982), and the main knickpoint is therefore
404 located at the hinge line 2 (the shelf-break) which also corresponds to the first development of forced falling
405 stage system tract of the MSC (Leroux *et al.*, 2015a, b). The model highlights the initiation of retrogressive
406 erosion at the second geodynamic knickpoint (the shelf break), which quickly progresses landward from the
407 former Miocene shelf-edge to the edge of the Central Massif (Pyrenean-Languedocian rivers) or along the
408 Rhone-Bresse valley (Fig. 8b, stage 1-3) up to Lyon city.

409 Domain 2a (GOL) can be compared to the VB basin area/VB-MB transition, which records the lowest
410 MSC base-level and early relative sea-level rise. Around the Km3 area, a minimum of four successive marine
411 incisions are observed in the UU deposits (Fig. 3, section e), implying (1) a composite refilling for the trans-VB
412 valley system and (2) preservation of the latter in the sense of Boyd *et al.*, (2006). If the UU are mainly developed
413 along the main channel (~0.3 twt thick) few deposits are observed on both sides of the channel, involving a
414 partial/complete reshaping of S20 erosional surface. This observation may be related to other morphological
415 features, such as the general extent of the smooth surface along the Catalan and domain 2b of the LPB (Bache
416 *et al.*, 2009, 2012; Garcia *et al.*, 2011; this study) (Fig. 6). This tends to favour a similar genesis during a relative
417 slow sea-level rise (Fig. 8, stage 4), the rough surface being eroded by wave action (Cattaneo and Steel, 2003;
418 Bache *et al.*, 2012, 2015) and only preserved upstream by the later rapid sea-level rise closing the Messinian
419 event.

420 We thus propose that domain 2b and VB basin area/VB-MB transition are equivalent morphological domains
421 which both record the lowest MSC sea-level. Significant lateral spacing between each morphological knickpoint
422 has provided better stratigraphic and morphological observation for the VB. As the VB record the whole
423 Messinian palaeo-Ebro incised valley, the Ebro paradox disappears if the length of Messinian rivers are
424 measured from MSC paleo-shorelines at the CFZ area, and not from pre-Messinian or present-day shorelines
425 (Fig. 7).

426 At the MSC paroxysm, the trans-VB incised valley system watershed would include the Valencia Basin and its
427 borders (55 000 km²; including the Betic-influenced southwest area, its mountainous borders (southern part
428 of the Catalan Range) and at least the eastern part of the Ebro Basin (? < Ebro watershed < 85 000 km²).
429 However, our result cannot confirm or infirm a pre-Messinian proto-Ebro hypothesis. Stratigraphic and
430 thermochronological interpretations path suggest a pre-Messinian opening of the Ebro Basin (Fillon *et al.*,
431 2012; Cameselle *et al.*, 2013) with a single proto-Ebro river or multiple mountainous rivers cutting across the
432 CCR. These models need to be confirmed by an assessment of offshore sedimentary volumes during Miocene,
433 Messinian and Pliocene-Quaternary times that would lead to a better estimate of the paleo-drainage area
434 evolution before/after the opening of the EB.

435 The NBFZ sill is overloaded by igneous pulses starting during the LU deposition and during Pliocene-
436 Quaternary time (Fig. 9; this was also observed onshore by Marti *et al.*, 1992; Araña *et al.*, 1983). Recent studies
437 have linked this Messinian magmatic pulse to the Messinian desiccation (Sternai *et al.*, 2017) or to a more
438 global kinematic re-organization (Leroux *et al.*, 2018). Whatever the lithospheric processes implied, the Ebro
439 incised-fluvial system constrained by the CCR and by the CFZ confirms the strong influence of VB-MB-LPB
440 margin structural segmentation on the development of the Messinian Ebro fluvial system, and more generally
441 on the whole Neogene sedimentological evolution.

443 5. Conclusion

444 Extending the Cameselle *et al.* (2014) results, we have identified and characterized along the Valencia, Menorca
445 and towards Liguro-Provence basins a 270 km long Messinian fluvial valley-incision - from the Messinian
446 shoreline to the CCR - as well as the spatial distribution of the related distal detrital deposits. The Ebro
447 Messinian erosional system now displays the same order of incised river length as the Rhone, resolving the
448 paradoxal relationship between the present-day fluvial drainage area and the Messinian fluvial system of
449 Babault *et al.*, (2006). Following our interpretation, the Ebro Basin and Mediterranean Sea were connected at
450 least at the MSC sea-level drop. Only detailed sedimentary fluxes analysis could confirm or infirm a pre-
451 Messinian connection between the Ebro Basin and the Mediterranean Sea.

452 The segmentation and nature of the substratum triggered the formation of knickpoints due to differential
453 subsidence between the shallow VB, the transitional MB and the deep LPB, and controlled fluvial processes
454 and erosion during the MSC sea-level drop. These knickpoints induced step-by-step major regressive-
455 retrogressive fluvial erosional processes which shift through time during sea-level drop. This work highlights
456 the general major relationship between kinematic, subsidence evolution, base-level fall and depositional
457 response particularly well expressed during the outstanding Messinian Salinity Crisis event.

458
459
460
461
462
463
464
465
466
467
468
469
470
471
472
473
474
475
476
477
478
479
480
481
482
483
484
485
486
487
488
489

Acknowledgments

This work was co-funded by a grant from the French government under the program "Investissements d'Avenir" the "Laboratoire d'Excellence" LabexMER (ANR-10-LABX-19), and ISBLUE (ANR-17-EURE-0015) and by a grant from the Regional Council of Brittany. It was further supported by CNRS and IFREMER, with additional support from the French Actions-Marges program (JL Rubino & P. Unternehr) and the GRI Méditerranée (Groupement Recherche et Industrie TOTAL-UPMC). The Data base was built thanks to the SIGEOF spanish site, to academic cruises from France including PROGRES, AMED-SARDINIA, SEEPGOL, VALSIS) and Spain. Additional industrial seismic lines were provided by Schlumberger. The biostratigraphic studies and re-evaluations were performed by biostratigraphers from TOTAL. The authors acknowledge the fruitful and constructive reviews by Antonio Pedrera, Agnes Maillard and two anonymous reviewers, as well as those from the editor Liviu Matenco that greatly improved the manuscript.

References

- Afilhado, A., Moulin, M., Aslanian, D., Schnürle, P., Klingelhoefer, F., Nouzé, H., Rabineau, M., Leroux, E., and Beslier, M.-O., 2015. Deep crustal structure across a young passive margin from wide-angle and reflection seismic data (The SARDINIA Experiment) - II. Sardinia's margin. *Bulletin de la société géologique de France*, 186, 331-351.
- Amblas, D., Canals, M., Urgeles, R., Lastras, G., Liqueste, C., Hughes-Clarke, J.E., Casamor, J.L., Calafat, A.M., 2006. Morphogenetic mesoscale analysis of the northeastern Iberian margin, NW Mediterranean Basin. *Marine Geology* 234, 3-20.
- Amblas, D., Gerber, T.P., Canals, M., Pratson, L.F., Urgeles, R., Lastras, G., and Calafat, A.M., 2011. Transient erosion in the Valencia Trough turbidite systems, NW Mediterranean Basin. *Geomorphology*, 130 (3-4), 173-184.
- Araña, V., Aparicio, A., Martín Escorza, C., García Cacho, L., Ortiz, R., Vaquer, R., Barberi, F., Ferrara, G., Albert, J., and Gassiot, X., 1983. El volcanismo neogeno-cuaternario de Catalunya: caracteres estructurales, petrologicos y geodinámicos. *Acta Geologica Hispanica*, 28, 1-17.
- Arche, A., G. Evans, and Clavell, E., 2010. Some considerations on the initiation of the present SE Ebro river drainage system: Post- or pre-Messinian? *Journal of Iberian Geology*, 36 (1), 73-85.
- Babault, J., Loget, N., Van Den Driessche, J., Castelltort, S., Bonnet, S., Davy, P., 2006. Did the Ebro basin connect to the Mediterranean before the Messinian salinity crisis? *Geomorphology*, 81, 155-165.

- 490 Bache, F., 2008. Evolution Oligo-Miocène des marges du micro océan Liguro-Provençal. Thèse d'Etat.
491 Université de Bretagne Occidentale, Brest, 1-328.
- 492 Bache, F., Olivet, J.L., Gorini, C., Rabineau, R., Baztan, J., Aslanian, D., and Suc, J.P., 2009. Messinian
493 erosional and salinity crises: view from the Provence basin (Gulf of Lions, Western Mediterranean). *Earth
494 and Planetary Science Letters*, 286, 139-157.
- 495 Bache, F., Olivet, J.L., Gorini, C., Aslanian, D., Labails, C., Rabineau, M., 2010. Evolution of rifted
496 continental margins: the cases of the Gulf of Lions (western Mediterranean basin). *Earth and Planetary
497 Science Letters*, 292, 345-356.
- 498 Bache, F., Gargani, J., Suc J.-P., Gorini, C., Rabineau, M., Popescu, S.M., Leroux, E., Do Couto, D., Jouannic,
499 G., Rubino, J.-L., Olivet, J.-L., Clauzon, G., Dos Reis, A., and Aslanian, D., 2015. Messinian evaporite
500 deposition during sea level rise in the Gulf of Lion (Western Mediterranean). *Marine and Petroleum
501 Geology*, 66, 262-277.
- 502 Bache, F., Popescu, S.-M., Rabineau, M., Gorini, C., Suc, J.-P., Clauzon, G., Olivet, J.-L., Rubino, J.-L., Melinte-
503 Dobrinescu, M.C., Estrada, F., Londeix, L., Armijo, R., Meyer, B., Jolivet, L., Jouannic, G., Leroux, E.,
504 Aslanian, D., Dos Reis, A.T., Mocochain, L., Dumurdžanov, N., Zagorchev, I., Lesić, V., Tomić, D.,
505 Çığatay, M.N., Brun, J.-P., Sokoutis, D., Csato, I., Uçarkus, G., Çakir, Z., 2012. A two-step process for
506 the reflooding of the Mediterranean after the Messinian Salinity Crisis. *Basin Research*, 24, 125-153.
- 507 Bache, F., Sutherland, R., and King, P.R., 2014. Use of ancient wave-ravinement surfaces to determine
508 paleogeography and vertical crustal movements around New Zealand. *New Zealand Journal of Geology
509 and Geophysics* 57, 459-467.
- 510 Bailey, H.W., Gallagher, L., Woodhouse, B., 2008. Biostratigraphy of the Well Fornax-Offshore, Spain, 12 pp.
511 Unpublished biostratigraphic report.
- 512 Balázs, A., Granjeon, D., Matenco, L., Sztanó, O., Cloetingh, S., 2017. Tectonic and climatic controls on
513 asymmetric half-graben sedimentation: inferences from 3-D numerical modelling. *Tectonics*, 36, 2123-
514 2141.
- 515 Bartrina, M.T., Cabrera, L.L., Jurado, M.J., Guimera, J., and Roca, E., 1992. Cenozoic evolution of the central
516 Catalan margin (Valencia Trough, Western Mediterranean). *Geology and Geophysics of the Valencia
517 Trough, Western Mediterranean. Tectonophysics*, 203, 219-248.
- 518 Baztan, J., Berné, S., Olivet, J.-L., Rabineau, M., Aslanian, D., Gaudin, M., Réhault, J.-P., and Canals, M.,
519 2005. Axial incision: the key to understand submarine canyon evolution (in the western Gulf of Lion).
520 *Marine and Petroleum Geology*, 22 (6-7), 805-826.

521 Bessais, E., 1984. Etude palynologique du Pliocène du sondage Tarragona E2. Rapport de stage D.E.A. Univ.
522 Sc. Tech. Languedoc, Montpellier, 21 pp.

523 Bessais, E. and Cravatte, J., 1988. Pliocène Vegetational ecosystems in South Catalonia, latitudinal variations
524 in the Northwest Mediterranean Region. *Geobios*, 21, 49-63.

525 Boyd, R., Dalrymple, R.W., and Zaitlin, B.A., 2006. Estuarine and Incised-Valley facies model. *SEPM special*
526 *publication*, 84, 171-235.

527 Comeselle, A.L., Urgeles, R., De Mol, B., Camerlenghi, A., and Canning, J.C., 2014. Late Miocene sedimentary
528 architecture of the Ebro Continental Margin (Western Mediterranean): implications to the Messinian
529 Salinity Crisis. *International Journal of Earth Science (Geol Rundsch)*, 1-18.

530 Comeselle, A.L., and Urgeles, R., 2015. Large-scale margin collapse during Messinian early sea-level drawdown:
531 the SW Valencia trough, NW Mediterranean. *Basin Research*, 29 (S1), 576-595.

532 Canals, M., Casamor, J.L., Lastras, G., Monaco, A., Acosta, J., Berné, S., Loubrieu, B., Weaver, P.P.E. and
533 Grehan, A., 2004. The role of canyons in strata formations. *Oceanography*, 17 (4), 81-91.

534 Canals et al., 2013. Integrated study of Mediterranean deep canyons: novel results and future challenges.
535 *Progress in Oceanography*, 118, 1-27.

536 Cattaneo, A. and Steel, R.J., 2003. Transgressive deposits: a review of their variability. *Earth-Science Reviews*,
537 62, 187-228.

538 Catuneanu, 2006. *Principles of sequence stratigraphy*. Amsterdam, The Netherlands, Elsevier. 375 pp.

539 Catuneanu, O., Galloway, W.E., Kendall, C.G.S.C., Miall, A.D., Posamentier, H.W., Strasser, A., Tucker,
540 M.E., 2011. Sequence stratigraphy: methodology and nomenclature. *Newslett. Stratigr.* 44 (3), 173-245.

541 CIESM, 2008. The Messinian Salinity Crisis from mega-deposits to microbiology – A consensus report. N° 33
542 in *CIESM Workshop Monographs* (F. Briand, Ed.), CIESM Publisher, Monaco, 168 pp.

543 Clauzon, G., 1982. Le canyon Messinien du Rhône : une preuve décisive du “desiccated deep-basin model”
544 (Hsü, Cita and Ryan, 1973). *Bull. Soc. Géol. Fr.*, 24 (3), 597-610.

545 Clauzon, G., 1999. L’impact des variations eustatiques du bassin de Méditerranée occidentale sur l’orogène
546 alpin depuis 20 Ma (In French). *Etudes Géogr. Phys.*, 28, 33-40.

547 Clauzon, G., Suc, J.-P., Gautier, F., Berger, A., Loutre, M.-F., 1996. Alternate interpretation of the Messinian
548 salinity crisis: Controversy resolved? *Geology*, 24, 363-366.

549 Clauzon, G., Suc, J.-P., Do Couto, D., Jouannic, G., Melinte-Dobrinescu, M.C., Jolivet, L., Quillévéré, F.,
550 Lebret, N., Mocochain, L., Popescu, S.-M., Martinell, J., Doménech, R., Rubino, J.-L., Gumiaux, C.,
551 Warny, S., Bellas, S.M., Gorini, C., Bache, F., Rabineau, M., Estrada, F., 2015. New insights on the

552 Sorbas Basin (SE Spain): The onshore reference of the Messinian Salinity Crisis. *Marine and Petroleum*
553 *Geology*, 66, 71–100.

554 Clavell E. and Berastegui X., 1991. Petroleum geology of the Gulf of València. Generation, accumulation, and
555 production of Europe's hydrocarbons (Ed. A.M. Spencer), Special Publication of the European
556 Association of Petroleum Geoscientists, 1, 355-368.

557 Costa, E., Garcés, M., Lopez-Blanco, M., Beamud, E., Gomez-Paccard, M., and Larrasoaña, J. C., 2010. Closing
558 and continentalization of the South Pyrenean foreland basin (NE Spain): magnetochronological
559 constraints. *Basin Research*, 22, 904-917.

560 Cravatte, J., 1980, Etude microstratigraphique du Miocène et essai de corrélations entre les forages de Te-2,
561 Garraf 1, BMB-1, BMC-1 et BME-1: Rapport confidentiel, total Direction fonctionnelle Exploration,
562 département Laboratoires Exploration, p. 1-16.

563 Del Olmo, W.M., 2011. The Messinian in the Gulf of Valencia and Alboran Sea (Spain): paleogeography and
564 paleoceanography implications. *Revista de la Sociedad Geológica de España*, 24, 1-22.

565 Do Couto, D., 2014. Evolution geodynamique de la Mer d'Alboran par l'étude des bassins sédimentaires.
566 Thèse de doctorat de l'Université Pierre et Marie Curie, 554 pp.

567 Escutia, C., Maldonado, A., 1992. Paleogeographic implications of the Messinian surface in the Valencia
568 trough, northwestern Mediterranean Sea. In: Banda, E., Santanach, P. (Eds.), *Geology and Geophysics of*
569 *the Valencia Trough, Western Mediterranean*. *Tectonophysics*, 203, 263–284.

570 Etheve, N., Frizon de Lamotte, D., Mohn, G., Martos, R., Roca, E., and Blanpied, C., 2016. Extensional vs
571 contractional Cenozoic deformation in Ibiza (Balearic promontory, Spain): Integration in the West
572 Mediterranean back-arc setting. *Tectonophysics*, 682, 35-55.

573 Etheve, N., Mohn, G., Frizon de Lamotte, D., Roca, E., Tugend, J., and Gomez-Romeu, J., 2018. Extreme
574 Mesozoic Crustal thinning in the eastern Iberia margin: the example of the Columbrets basin (Valencia
575 trough). *Tectonics*, 37 (2), 636-662.

576 Evans, D.J., Peter, C.K., Price, R.J., 1978. Biostratigraphy and depositional environments over the interval 450
577 m to 4492 m (T.D.), together with petrographic descriptions of samples between 3620 m to 4190 m in
578 the Union Texas Espana Inc. Benicarlo C-1 well, offshore Spain, Robertson Research (North America)
579 Limited, unpublished Exploration Report n° 194, 61 pp.

580 Fidalgo-González, L., 2001. Kinematic evolution of the North Atlantic ocean: implication of the intraplate
581 deformation. Thèse de doctorat de l'Université de Bretagne Occidentale, Brest, 1-477.

582 Fillon, C., Gautheron, C., and van der Beek, P., 2013. Oligocene–Miocene burial and exhumation of the
583 Southern Pyrenean foreland quantified by low-temperature thermochronology. *Journal of the Geological*
584 *Society*, 170, 67-77.

585 Flecker, R., Krijgsman, W., Capella, W., de Castro Martins, C., Dmitriev, E., Mayser, J.P., Marzocchu, A.,
586 Modestu, S., Ochoa, D., Simon, D., Tulbure, M., van der Berg, B., van der Schee, M., de Lange, G.,
587 Ellam, R., Govers, R., Gutjah, M., Hilgen, F., Kouwenhoven, T.J., Lofi, J., Meijer, P., Sierro, F.J., Bachiri,
588 N., Barhoun, N., Alami, A.C., Chacon, B., Flores, J.A., Gregory, J., Howard, J., Lunt, D., Ochoa, M.,
589 Pancost, R., Vincent, S., and Yousfi, M.Z., 2015. Evolution of the Late Miocene Mediterranean–Atlantic
590 gateways and their impact on regional and global environmental change. *Earth-Science Reviews*, 150,
591 365-392.

592 Frey-Martinez, J., Cartwright, J.A., Burgess, P.M., and Vicente-Bravo, J., 2004. 3D seismic interpretation of the
593 Messinian Unconformity in the Valencia Basin, Spain: 3D Seismic Technology: Application to the
594 Exploration of Sedimentary Basins. (Ed. by R.J. Davies, J.A. Cartwright, S.A. Stewart, M. Lappin & J.R.
595 Underhill). *Memoirs of the Geological Society*, London, 29, 91-100.

596 Garcia, M., Maillard, A., Aslanian, D., Rabineau, M., Alonso, B., Gorini, C., and Estrada, F., 2011. The
597 Catalan margin during the Messinian Salinity Crisis: Physiography, morphology and sedimentary record.
598 *Marine Geology*, 284, 158-174.

599 Garcia-Castellanos, D., and Larrasoana, J.C., 2015. Quantifying the post-tectonic topographic evolution of
600 closed basins: The Ebro basin (northeast Iberia). *Geology*, 43 (8), 663-667.

601 Gorini, C., Montadert, L., and Rabineau, M., 2015. New imaging of the salinity crisis: Dual Messinian
602 lowstand megasequences recorded in the deep basin of both the eastern and western Mediterranean.
603 *Marine and Petroleum Geology*, 66, 1-17.

604 Goswami, R., Mitchell, N.C., Brocklehurst, S.H. and Argnani, A., 2016. Linking subaerial erosion with
605 submarine geomorphology in the western Ionian Sea (south of the Messina Strait), Italy. *Basin Research*,
606 29, 641-658.

607 Gradstein, F.M., Ogg, J.G., Schmitz, M.D., Ogg, G.M., (eds.) 2012. *The Geological Time Scale 2012*, Elsevier,
608 Amsterdam, 1144 pp.

609 Grimaud, J.-L., Paola, C. and Voller, V., 2016. Experimental migration of knickpoints: influence of style of
610 base-level. *Earth-Surface Dynamics*, 4, 1-11.

611 Gueguen, E., Doglioni, C., and Fernandez, M., 1998. On the post-25 Ma geodynamic evolution of the western
612 Mediterranean. *Tectonophysics*, 298, 259-269.

613 Guennoc, P., Gorini, C., and Mauffret, A., 2000. Histoire géologique du Golfe du Lion et cartographie du rift
614 oligo-aquitainien et de la surface messinienne. *Géologie de la France*, 3, 67-97.

615 Helland-Hansen, W. & Hampson, G. 2009. Trajectory analysis: concepts and application. *Basin Research*, 21
616 (5), 454-483.

617 Hunt, D. and Tucker, M. E., 1992. Stranded parasequences and the forced regressive wedge systems tract:
618 deposition during base-level fall, *Sedimentary Geology*, 81, 1-9.

619 Iaccarino, S., Premoli Silva, I., Biolzi, M., Foresi, L.M., Lirer, F., Turco, E., Petrizzo, M.R., 2007. Practical
620 manual of Neogene planktonic foraminifera. Biolzi, M., Iaccarino, S., Turco, E., Checconi, A., Rettori,
621 R., eds., Univ. Perugia-Parma-Milano, 131 pp.

622 Jolivet, L., C. Gorini, Smit, J., and Leroy, S., 2015. Continental breakup and the dynamics of rifting in back-
623 arc basins: The Gulf of Lion margin. *Tectonics* 34 (4): 2014TC003570.

624 Koss, J.E., Ethridge, F.G., Schumm, S.A., 1994. An experimental study of the effects of base-level change on
625 fluvial, coastal plain and shelf systems. *Journal of Sedimentary Petrology*, 64, 90-98.

626 Krijgsman, W., Langereis, C.G., Zachariasse, W.J., Boccaletti, M., Moretti, G., Gelati, R., Iaccarino, S., Papani,
627 G., and Villa, G., 1999. Late neogene evolution of the Taza–Guercif Basin (Rifian Corridor, Morocco)
628 and implications for the Messinian salinity crisis. *Marine Geology*, 153, 147–160.

629 Leever, K.A., Matenco, L., Garcia-Castellanos, D., and Cloetingh, S., 2010. The evolution of the Danube
630 gateway between Central and Eastern Paratethys (SE Europe): Insight from numerical modelling of the
631 causes and effects of connectivity between basins and its expression in the sedimentary record.
632 *Tectonophysics*, 502, 175-195.

633 Leroux, E., Aslanian, D., Rabineau, M., Granjeon, D., Gorini, C., and Droz, L., 2015a. Sedimentary markers
634 in the Provençal Basin (western Mediterranean): a window into deep geodynamic processes. *Terra Nova*,
635 27, 122-129.

636 Leroux, E., Rabineau, M., Aslanian, D., Gorini, C., Bache, F., Moulin, M., Pellen, R., Granjeon, D., and
637 Rubino, J.-L., 2015b. Post-rift evolution of the Gulf of Lion margin tested by stratigraphic modelling.
638 *Bulletin de la Société Géologique de France*, 186, 291-308.

639 Leroux et al., 2017 (Leroux, E., Rabineau, M., Aslanian, D., Gorini, C., Bache, F., Robi, C., Droz, L., Moulin,
640 M., Poort, J., Rubino, J.-L., and Suc, J.P., 2017. High-resolution evolution of terrigenous sediment yields
641 in the Provence Basin during the last 6 Ma: relation with climate and tectonics. *Basin Research*, 29, 305-
642 339.

643 Leroux, E., Aslanian, D., Rabineau, M., Pellen, R., and Moulin, M., 2018. The late Messinian event: a
644 worldwide tectonic upheaval. *Terra Nova*, 30 (3), 207-214.

645 Lirer, F., Iaccarino, S., 2011. Mediterranean Neogene historical stratotype sections and Global Stratotype
646 Section and Points (GSSP): state of the art. *Ann. Naturhist. Mus. Wien*, 113(A), 67-144.

647 Lofi, J., Sage, F., Deverchère, J., Loncke, L., Maillard, A., Gaullier, V., Thinon, I., Gillet, H., Guennoc, P., and
648 Gorini, C., 2011. Refining our knowledge of the Messinian Salinity crisis records in the offshore domain
649 through multi-site seismic analysis. *Bulletin de la Société Géologique de France*, 182, 163-180.

650 Lofi, J., Camerlenghi, A., Aloisi, G., -Maillard, A. Garcia-Castellanos, D., Huebscher, C., Kuroda, J., 2017. The
651 DREAM IODP project to drill the Mediterranean Salt Giant on the balearic promontary, EGU.

652 Maillard, A., Mauffret, A., 1999. Crustal structure and rift genesis of the Valencia Trough (NW Mediterranean
653 Sea). *Basin Research*, 11, 357-379.

654 Maillard, A., Mauffret, A., 2006a. Relationship between erosion surfaces and Late Miocene Salinity Crisis
655 deposits in the Valencia Basin (Northwestern Mediterranean): evidence for an early sea-level fall. *Terra
656 Nova*, 18, 321-329.

657 Maillard, A., Gorini, C., Mauffret, A., Sage, F., Lofi, J., Gaullier, V., 2006b. Offshore evidence of polyphase
658 erosion in the Valencia Basin (Northwestern Mediterranean): scenario for the Messinian Salinity Crisis.
659 *Sedimentary Geology*, 188-189, 69-91.

660 Manzi, V., Gennari, R., Hilgen, F., Krijgsman, W., Lugli, S., Roveri, M., and Siorro, F.J., 2013. Age refinement
661 of the Messinian salinity crisis onset in the Mediterranean. *Terra Nova*, 25, 315-322.

662 Marti J., Mitjavila, J., Roca, E., Aparicio, A., 1992. Cenozoic magmatism of the Valencia through (western
663 Mediterranean): relationship between structural evolution and volcanism. *Tectonophysics*, 203, 145-165.

664 Mauffrey, M-A., Urgeles, R., Berné, S., Canning, J., 2017. Development of submarine canyons after the Mid-
665 Pleistocene Transition on the Ebroi margin, NW Mediterranean: The role of fluvial connections,
666 *Quaternary Science Reviews*, 158, 77-93.

667 Miall, A.D., 2013. *The Geology of Fluvial Deposits*, 4th corrected printing, 581 pp.

668 Mitchum R. & Vail P., 1977. Seismic stratigraphy and global changes of sea-level, part 7: Seismic Stratigraphic
669 Interpretation Procedure - In *Seismic Stratigraphy - Applications to hydrocarbon exploration*; Payton C.
670 E. (ed.): AAPG Mem. 26, Tulsa, Oklahoma, USA.

671 Moulin, M., Klingelhoefer, F., Afilhado, A., Aslanian, D., Schnurle, P., Nouzé, H., Rabineau, M., Beslier, M.-
672 O., and Feld, A., 2015. Deep crustal structure across a young passive margin from wide-angle and
673 reflection seismic data (The SARDINIA Experiment) - I. Gulf of Lion's margin. *Bulletin de la Société
674 Géologique de France*, 186, 309-330.

675 Olivet, J.L., 1996. La cinématique de la plaque Ibérique. *Bulletin des Centres de Recherches Exploration-
676 Production Elf-Aquitaine*, 20, 131-195.

677 Palcu, D.V., Golovina, L.A., Vernyhorova, Y.V., Popov, S.V., and Krijgsman, W., 2017. Middle Miocene
678 paleoenvironmental crises in Central Eurasia caused by changes in marine gateway configuration. *Global
679 and Planetary Change*, 158, 57-71.

680 Pellen, R., Aslanian, D., Rabineau, M., Leroux, E., Gorini, C., Silenziario, C., Blanpied, C., and Rubino, J.-L.,
681 2016. The Menorca Basin: a buffer zone between the Valencia and Liguro-Provençal Basins (NW
682 Mediterranean Sea). *Terra Nova*, 00, 1-16.

683 Pellen, R., Popescu, S.-M., Suc, J.-P., Melinte-Dobrinescu, M.C., Rubino, J.-L., Rabineau, M., Marabini, S.,
684 Loget, N., Casero, P., Cavazza, W., Head, M.J., and Aslanian, D., 2017. The Apennine foredeep (Italy)
685 during the latest Messinian: Lago Mare reflects competing brackish and marine conditions based on
686 calcareous nannofossils and dinoflagellate cysts. *Geobios*, 50 (3), 237-257.

687 Plint A. G., 1988. Sharp-based shoreface sequences and “offshore bars” in the Cardium Formation of Alberta:
688 their relationship to relative changes in sea level - In *Sea-level changes : an integrated approach* ; Wilgus
689 C. K., Hastings B. S. Et al. : SEPM Special Publication No. 42, Tulsa: p.357-370.

690 Rabineau, M., Berné, S., Aslanian, D., Olivet J.-L., Joseph, P., Guillocheau, F., Bourillet, J.-F., Ledrezen, E.,
691 Granjeon, D., 2005 : Sedimentary sequences in the Gulf of Lions : a record of 100,000 years climatic
692 cycles, *Marine and Petroleum Geology*, 22, 775-804.

693 Rabineau, M., Leroux, E., Bache, F., Aslanian, D., Gorini, C., Moulin, M., Molliex, S., Droz, L., Reis, T.D.,
694 Rubino, J.-L., and Olivet, J.-L., 2014. Quantifying subsidence and isostatic readjustment using
695 sedimentary paleomarkers, example from the Gulf of Lion. *Earth and Planetary Science Letters*, 388, 1-
696 14.

697 Rebesco, M., Hernandez-Molina, F.J., Van Rooij, D., and Wahlin, A., 2014. Contourites and associated
698 sediments controlled by deep-water circulation processes: state-of-the-art and future considerations.
699 *Marine Geology*, 352 (1), 111-154.

700 Roca, E., 2001. The Northwest Mediterranean Basin (Valencia Trough, Gulf of Lion and Liguro-Provençal
701 basins): structure and geodynamic evolution. *Peri-Tethyan Rift/Wrench Basins and Passive margins*, 186
702 (Ed. by P.A. Ziegler, W. Cavazza, A.H.F. Robertson & S. Crasquin-Soleau), pp. 671-706. *Peri-Tethys
703 Memoir 6, Mémoires du Muséum National d’Histoire Naturelle*, Paris.

704 Roca E. and Guimerà J., 1992. The Neogene structure of the eastern Iberian margin: structural constraints on
705 the crustal evolution of the Valencia trough (western Mediterranean). *Tectonophysics*, 203, 203-218.

706 Roure, F., Choukroune, P., Berastegui, X., Munoz, J.A., Villien, A., Matheron, P., Bareyt, M., Seguret, M.,
707 Camara, P., and Deramond, J., 1989. ECORS deep seismic data and balanced cross sections: geometric
708 constraints on the evolution of the Pyrenees. *Tectonics*, 8, 41-50.

- 709 Roveri, M., Flecker, R., Krijgsman, W., Lofi, J., Lugli, S., Manzi, V., Sierro, F.J., bertini, A., Camerlenghi, A.,
710 De Lange, G., Govers, R., Hilgen, F.J., Hübscher, C., Meijer, P.T., and Stoica, M., 2014, The Messinian
711 Salinity Crisis: Past and future of a great challenge for marine sciences: *Marine Geology*, 352, 25-58.
- 712 Séranne, M., 1999. The Gulf of Lion continental margin (NW Mediterranean) revisited by IBS: an overview.
713 in Durand, B., Jolivet, L., Horvath, F., and Seranne, M., eds., *The Mediterranean Basins: Tertiary*
714 *Extension within the Alpine Orogen*, Volume 156, Special publication, Geological Society of London,
715 p.15-36.
- 716 Sissingh, W., 2001. Tectonostratigraphy of the West Alpine Foreland; correlation of Tertiary sedimentary
717 sequences, changes in eustatic sea-level and stress regimes. *Tectonophysics*, 333, 361-400.
- 718 Slingerland, R., and Smith, N.D., 2004. River avulsions and their deposits. *Annual Review of Earth and*
719 *Planetary Sciences*, 32, 257-285.
- 720 Stampfli, G.M., and Hoëcker, C.F.W., 1989. Messinian palaeorelief from a 3D seismic survey in the Tarraco
721 concession area (Spanish Mediterranean Sea). *Geologie en Mijnbouw*, 68, 201-210.
- 722 Sternai, P., Caricchi, L., Garcia-Castellanos, D., Jolivet, L., Sheldrake, T.E., and Castelltort, S., 2017. Magmatic
723 pulse driven by sea-level changes associated with the Messinian salinity crisis. *Nature Geoscience*, 10,
724 783-787.
- 725 Suc, J.-P., Bertini, A., Combourieu-Nebout, N., Diniz, F., Leroy, S., Russo-Ermolli, E., Zheng, Z., Bessais, E.,
726 and Ferrier J., 1995. Structure of West Mediterranean vegetation and climate since 5.3 Ma. *Acta zool.*
727 *Cracov.*, 38 (1), 3-16.
- 728 Suc, J.-P., Clauzon, G., Bessedik, M., Leroy, S., Zheng, Z., Drivaliari, A., Roiron, P., Ambert, P., Martinell, J.,
729 Doménech, R., Matias, I., Julià, R., Anglada, R., 1992. Neogene and Lower Pleistocene in Southern
730 France and Northeastern Spain. *Mediterranean environments and climate. Cahiers Micropaléontol.*, 7
731 (1-2), 165-186.
- 732 Suc, J.-P., Popescu, S.-M., Do Couto, D., Clauzon, G., Rubino, J.-L., Melinte-Dobrinescu, M.C., Quillévéré, F.,
733 Brun, J.-P., Dumurdzanov, N., Zagorchev, I., Lesic, V., Tomic, D., Sokoutis, D., Meyer, B., Macalet, R.,
734 and Rifelj, H., 2015. Marine gateway vs. fluvial stream within the Balkans from 6 to 5 Ma. *Marine and*
735 *Petroleum Geology*, 66, 231-245.
- 736 Urgeles, R., Camerlenghi, A., Garcia-Castellanos, D., De Mol, B., Garcés, M., Vergés, J., Haslamk, I., and
737 Hardmank, M., 2011. New constraints on the Messinian sea level drawdown from 3D seismic data of
738 the Ebro Margin, western Mediterranean. *Basin Research*, 23, 123-145.

739 Vail, P.R., Mitchum, R.M., Todd, J.R.G., Widmier, J.M., Thompson, S., Sangree, J.B., Bubbs, J.N., Hatlelid,
740 W.G., 1977. In: Payton, C.E. (Ed.), *Seismic stratigraphy and global changes of sea level: Seismic*
741 *Stratigraphy - Applications to Hydrocarbon Exploration*. Mem. Am. Ass. Pertol. Geol., 26, 49–212.
742 Vasquez-Urbez, M., Arenas, C., Pardo, G., and Pérez-Rivarés, J., 2013. The effect of drainage reorganization
743 and climate on the sedimentologic evolution of intermontane lake systems: the final fill stage of the
744 Tertiary Ebro Basin (Spain). *Journal of Sedimentary Research*, 83, 562-590.

746 Figures

748 **Fig.1.** A Present-day NW Mediterranean physiographic areas **and** previously published major
749 physiographic features and seismic units assigned to the Messinian event (compiled from Stampfli and
750 Hoëcker, 1989; Frey-Martinez *et al.*, 2004; Maillard *et al.*, 2006a, b; Del Olmo, 2011; Garcia *et al.*, 2011; Urgeles
751 *et al.*, 2011; Bache *et al.*, 2009, 2015). Major geodynamic boundaries are represented in the Valencia-Menorca
752 Basin (VB-MB): C.F.Z. = Central Fracture Zone; N.B.F.Z. = North Balearic Fracture Zone) (Maillard and
753 Mauffret, 1999; Pellen *et al.*, 2016) and in the Liguro-Provence Basin (LPB): domain 1 = Unthinned
754 Continental Crust; domain 2a = Thinned Continental Crust.; domain 2b = Highly thinned Continental Crust;
755 domain 3 = Exhumed lower crust; domain 4 = Atypical oceanic crust) (Moulin *et al.*, 2015; Leroux *et al.*, 2015).

756 **Fig.2.** Map showing our new interpretation of the sedimentary units and main morphological
757 observations associated to the Messinian event in the VB-VM. The Messinian drainage network (in red) could
758 be followed from the shelf to the VB and up to the MB. Position of vertical sections a to f shown in black (see
759 Fig. 3).

760 **Fig.3.** Seismic sections a-f showing the morphological evolution of the trans-VB Messinian valley system,
761 its outlet and the related Messinian detrital and evaporitic deposits. The red marker symbolizes MES and S20
762 rough surface, the violet markers symbolize the smoother S21 surface at the outlet of the valley system.
763 Transect01 is a composite dip section converted in depth (see methods and supplementary figures for more
764 details) from the VB to the deep LPB. Note in particular the progressive downward shifts of top of units 12a
765 and 12c). Position of the profiles is given in Fig. 2.

766 **Fig. 4.** Detailed seismic section highlighting the development of a Miocene ante-MSC platform along
767 the Ebro-Tortosa area (section g) which mark Km2 knickpoint. The development of SU12a is associated to a
768 regressive surface of marine erosion (RSME) (section g) and to a major change in the origin of sediment supply
769 (section h). MES morphological region (section g) is deduced from Urgeles *et al.* (2011).

770 **Fig. 5.** Detailed seismic section highlighting the erosional truncations at the transition between the VB
771 and the MB domain (section i) and development of the progradational seismic units SU12c in the deep and
772 distal MB area (section j). We interpret this SU12c unit as the LST related to the MSC, it corresponds to the
773 most distal progradating detritic unit observed in the area.

774 **Fig. 6.** Correlation of seismic units and Well Benicarlo C1, for the Miocene to Pliocene deposits.
775 (Borehole position is shown on Figure 1 & 2). The right part of the figure shows the vertical records of the
776 concerned species, the horizontal lines indicate which level has been considered as corresponding to the first
777 or last appearance datum (FAD or LAD) of some of them. Biozones and related ages refer to Gradstein *et al.*
778 (2012). Caliper (blue curve) and Gamma Ray (red curve) are represented.

779 **Fig.7.** Simplified schematic section illustrating the role of multiple versus single knickpoints in
780 retrogressive erosion response during a relative sea level fall. **a, b, c** correspond to the rejuvenation phase of
781 the retrogressive erosion linked to the relative sea level successive falls (step 1, 2, 3).

782 **Fig.8.** Schematic and balanced cross section of the VB-MB and LPB (modified from Bache, 2008)
783 illustrating the impact of sills and sea-level drop on the fluvial valley system development and paleo-depositional
784 profile process during the Messinian event. During sea-level drop, erosion occurs both as regressive erosion of
785 the fluvial system but also as retrogressive erosion from more distal knickpoints (see text for further
786 explanation).

787 **Fig.9.** Detailed seismic section highlighting the magmatic pulse during the Lower Unit deposition and
788 Pliocene-Quaternary time at the Menorca Basin and Liguro-Provence Basin transition (North Balearic Fracture
789 Zone area) (Location and units color code as in Figs. 4 & 5).

792 SUPPLEMENTARY MATERIAL

793
794 **Supplementary material 1. A)** Time-depth velocity model used for the time to depth conversion of the
795 Transect01 using velocity information from boreholes (Benicarlo C1, Bocarte 1, Castellon G1, Tarragona D2
796 and Fornax 1) and ESP refraction data in the VB and GOL.

797 **Supplementary material 2.** Backstripping reconstruction along the regional Transect01 profile (in
798 depth). Input parameters for the VB domain include palaeobathymetry, age, and porosity of sedimentary
799 packages based on Urgeles *et al.* (2011). Rabineau *et al.* (2014) presented a new method to quantify post-rift
800 subsidence by direct use of sedimentary geometries. An estimated total subsidence value up to 960 m/Ma for

801 the deep LPB domain was estimated for Pliocene and Quaternary times ([Rabineau et al., 2014](#)) and applied to
802 the 2-D backstripping. MES, S20 and base of Halite surfaces were reported on Fig. 3. Q1, Q2, P1 and P2 are
803 respectively dated at 0.9, 1.8, 2.49 and 3.2 Ma following [Urgeles et al. \(2011\)](#) and [Leroux et al. \(2015b\)](#) studies.

804 **Supplementary material 3.** Summary of key seismic surfaces and units mapped across VB, MB, and LPB
805 areas in this study. Unit age estimation are from [Bache et al. \(2015\)](#) and [Gorini et al. \(2015\)](#).

806 **Supplementary material 4.** Short video illustrating the evolution of sea-level and paleogeographies in
807 the VB, MB and LPB between 6 and 5.20 Ma (using Placa 4D©ifremer software).

808

FIGURE 01

Previously published MSC physiography and deposit markers

Morphologic observations

- Early Pliocene ria area
- Relief > 300m
- Present-day Ebro and Rhone drainage area
- Known drainage network
- Supposed MESC valley
- Major geodynamic related knickpoint

Units

- Pre-rift substratum/ Miocene eroded unit
- Preserved Primary evaporite Unit
- MSC falling stage systems tract
- Bedded Unit
- Limit of the Lower Unit (LU)
- Mobile Unit (MU)
- Salt diapir area
- MU upper limit
- Limit of the Upper Unit (UU)

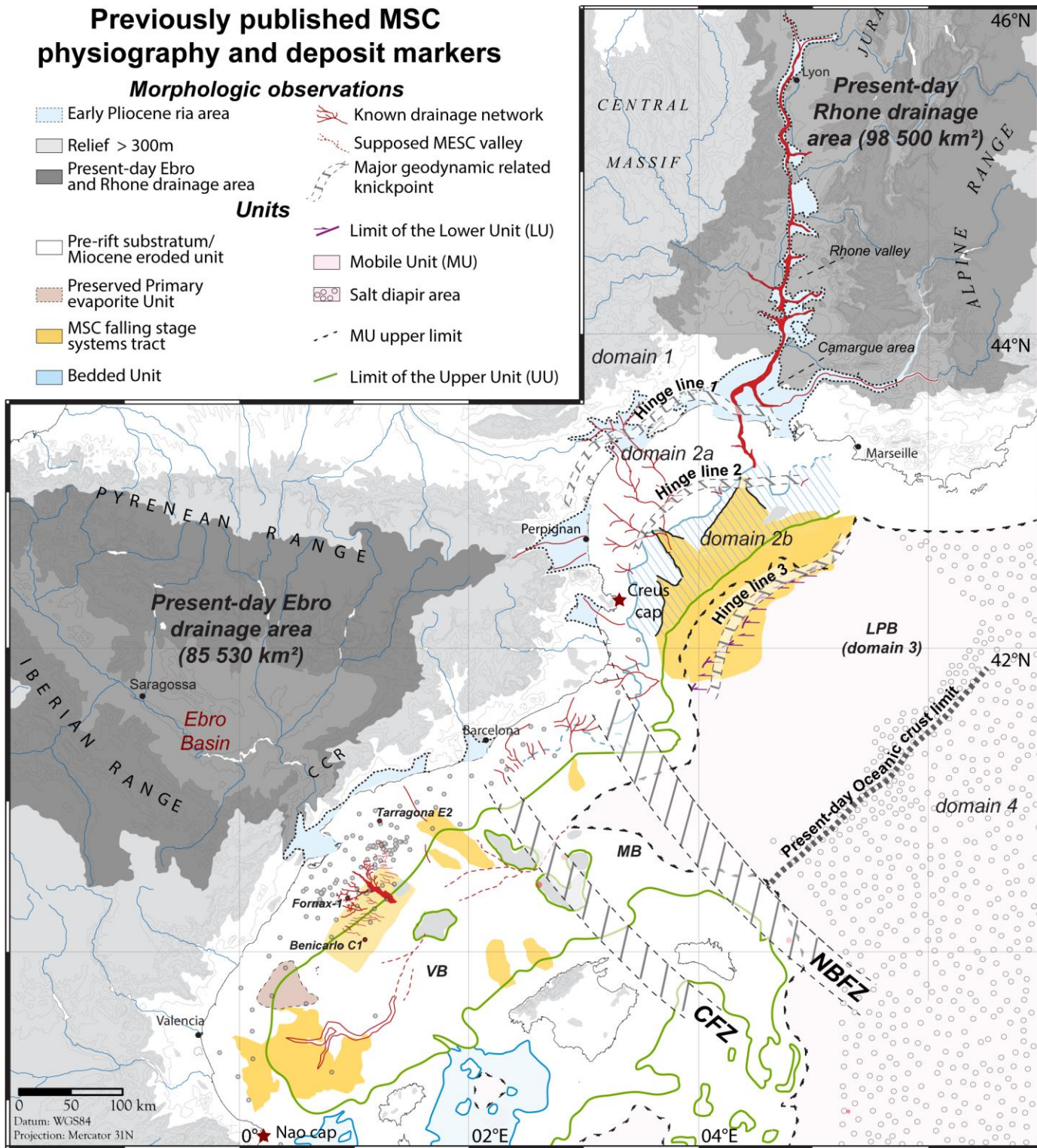
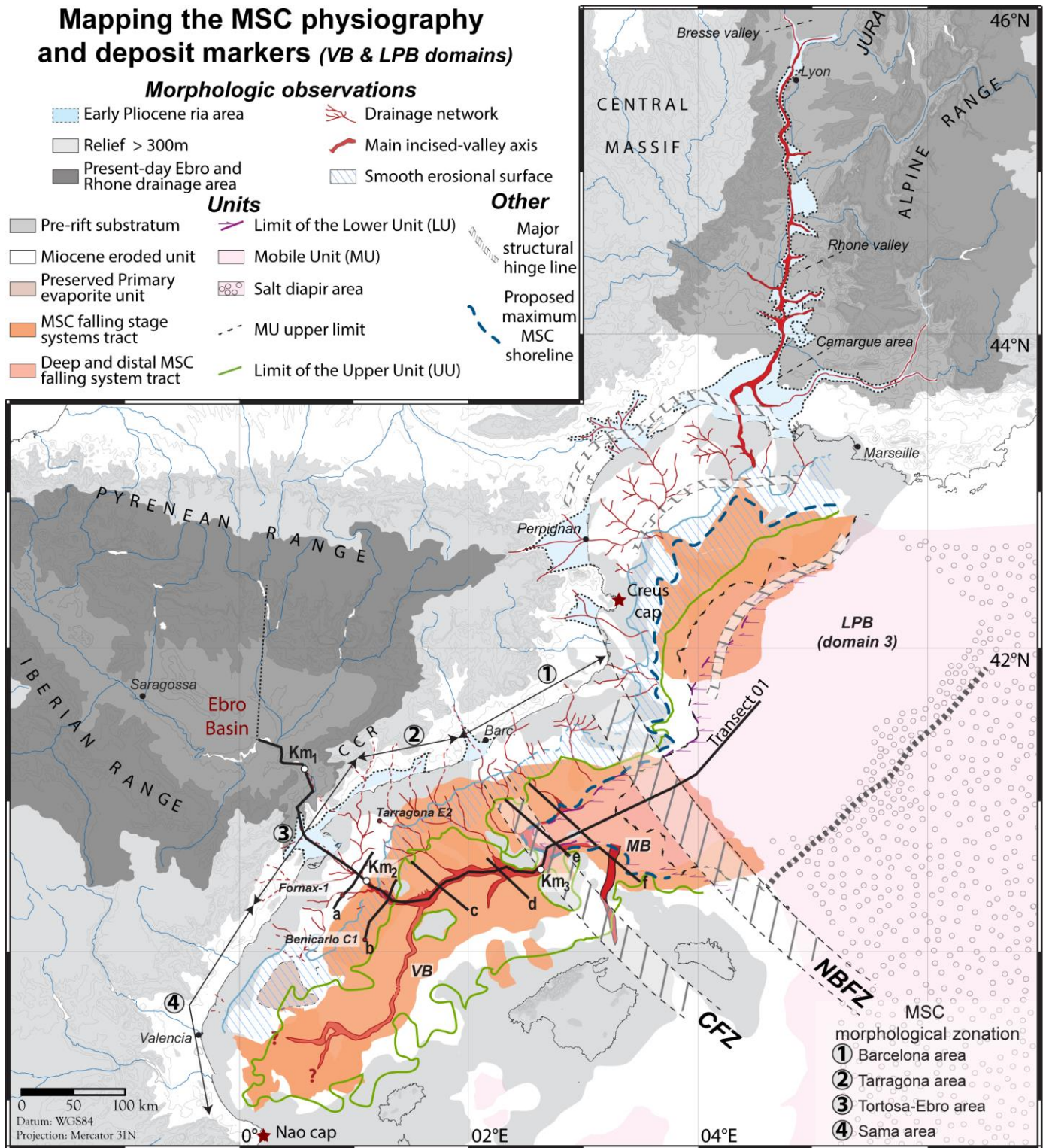
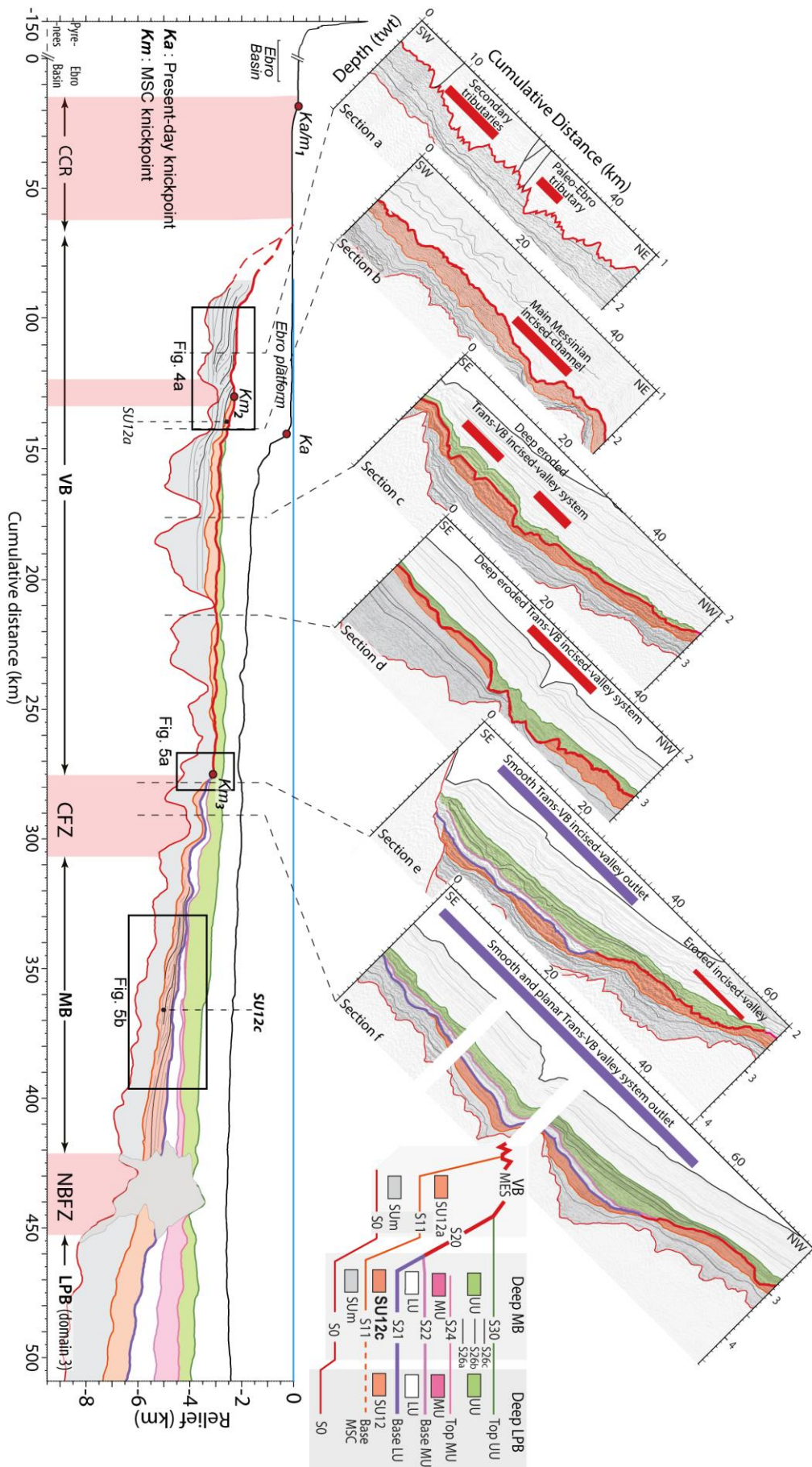


FIGURE 02



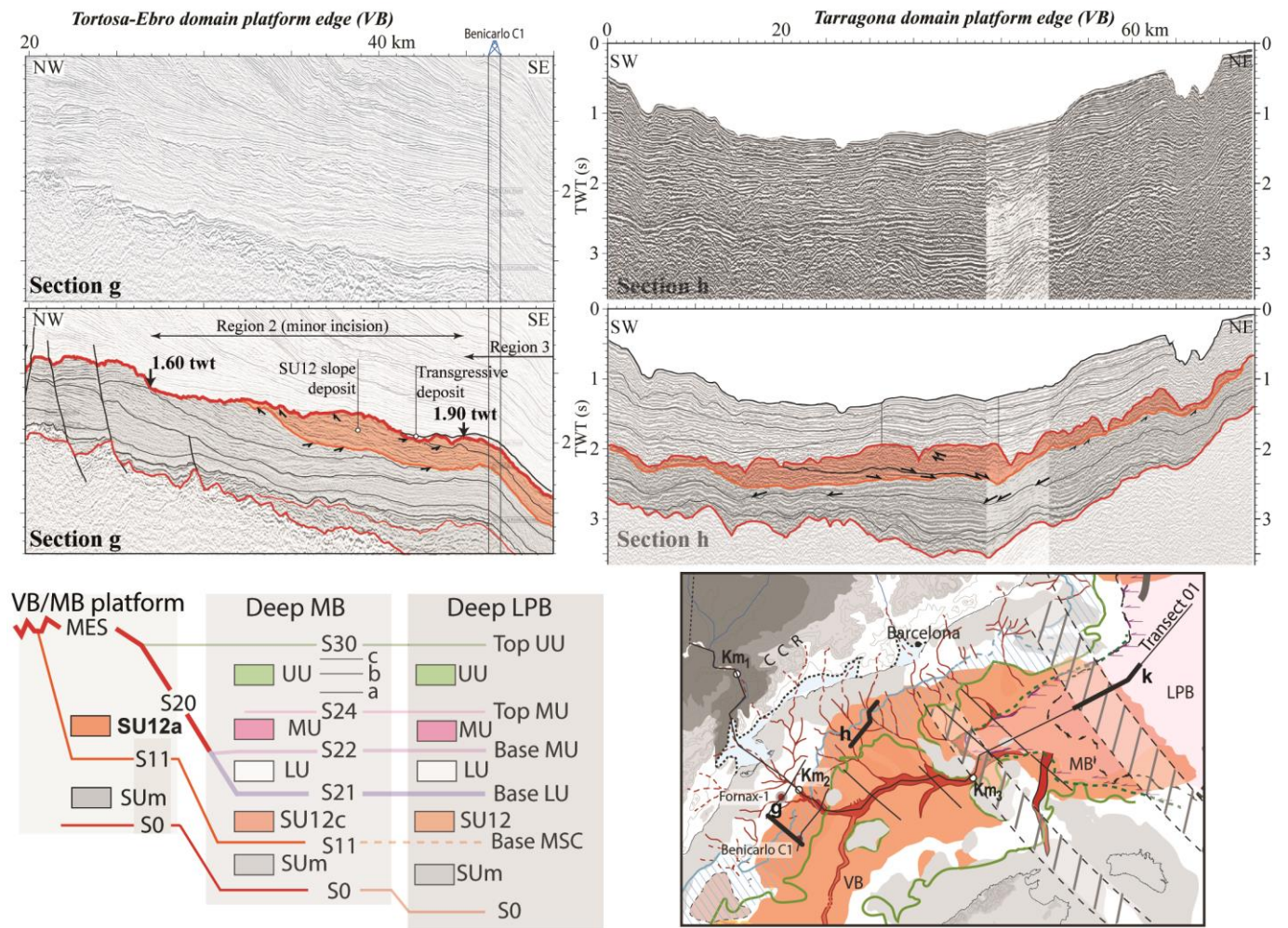
815
816

FIGURE 03



817

FIGURE 04



818

819

FIGURE 05

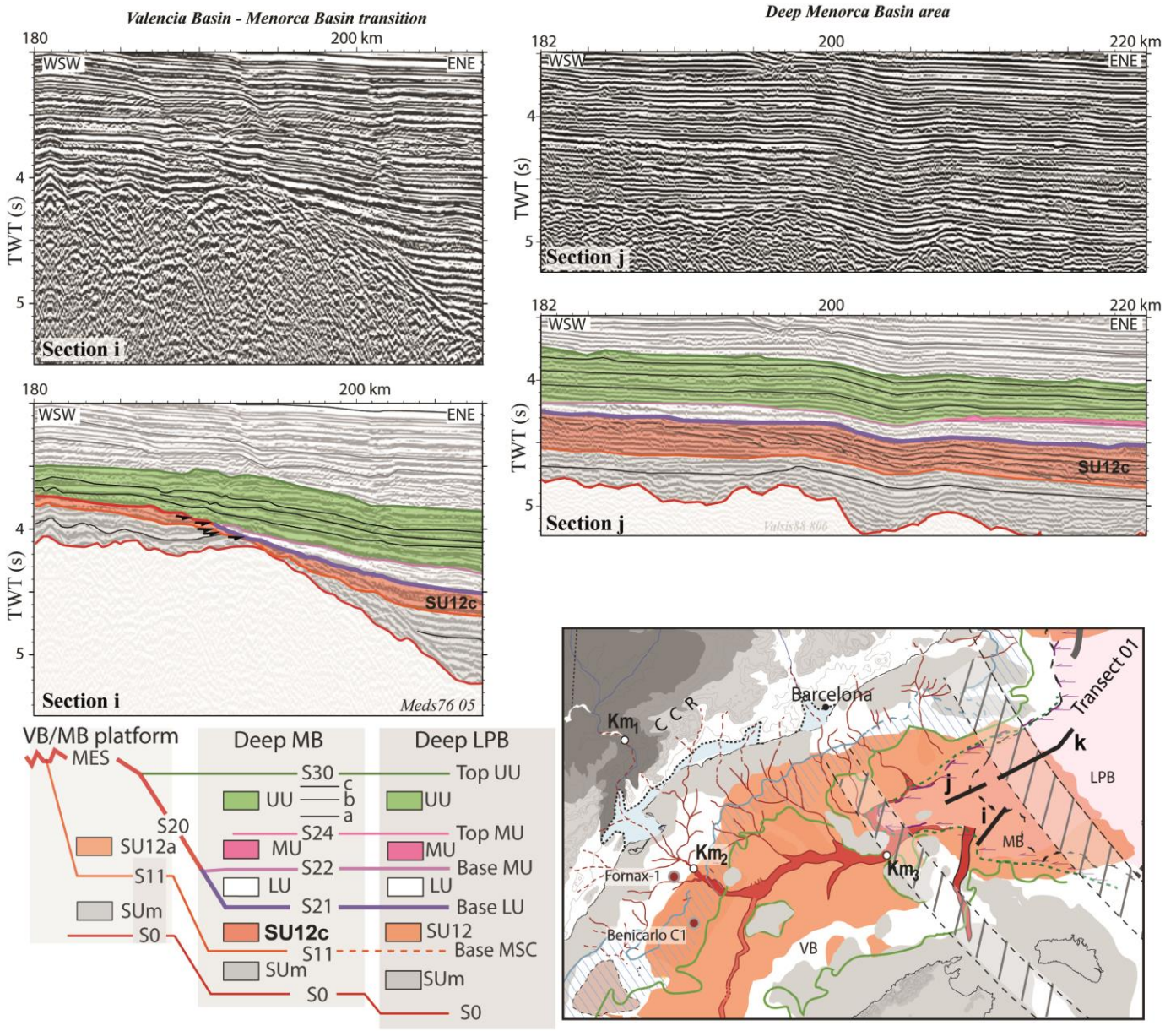
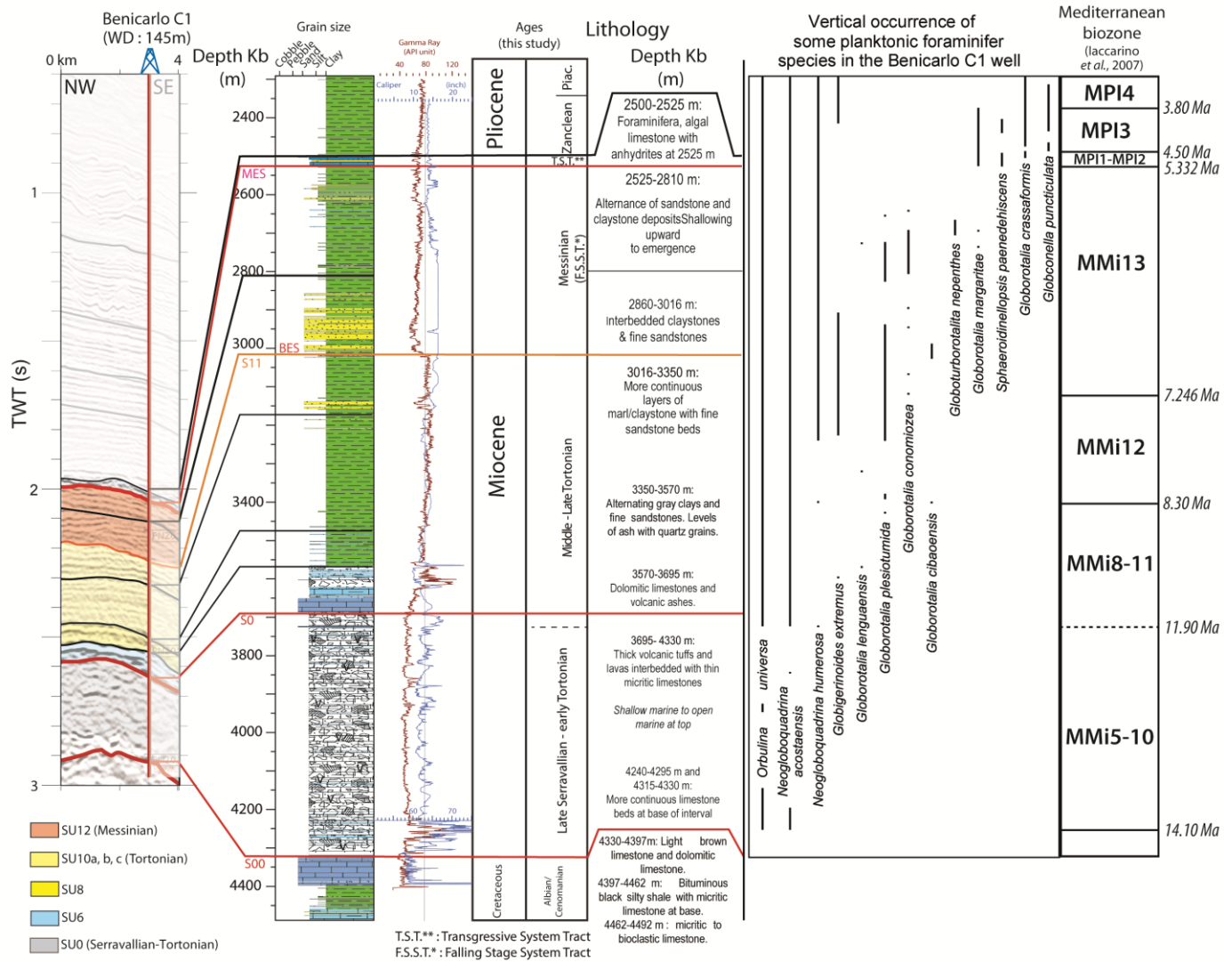


FIGURE 06



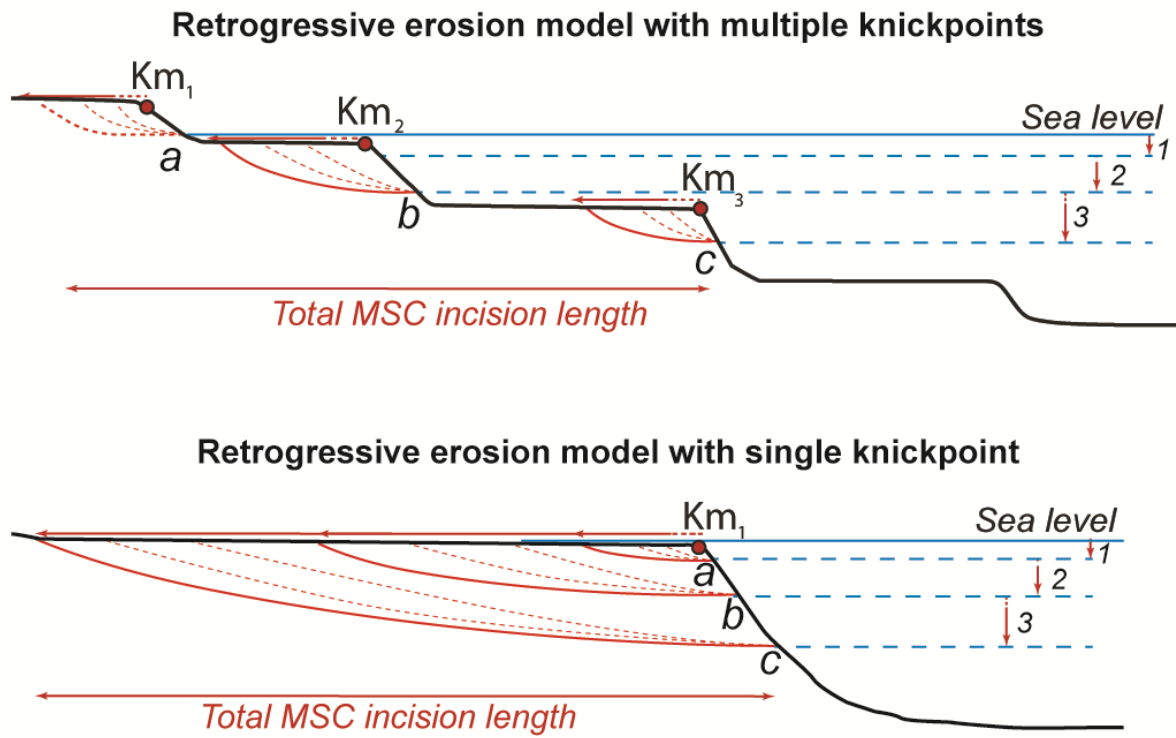
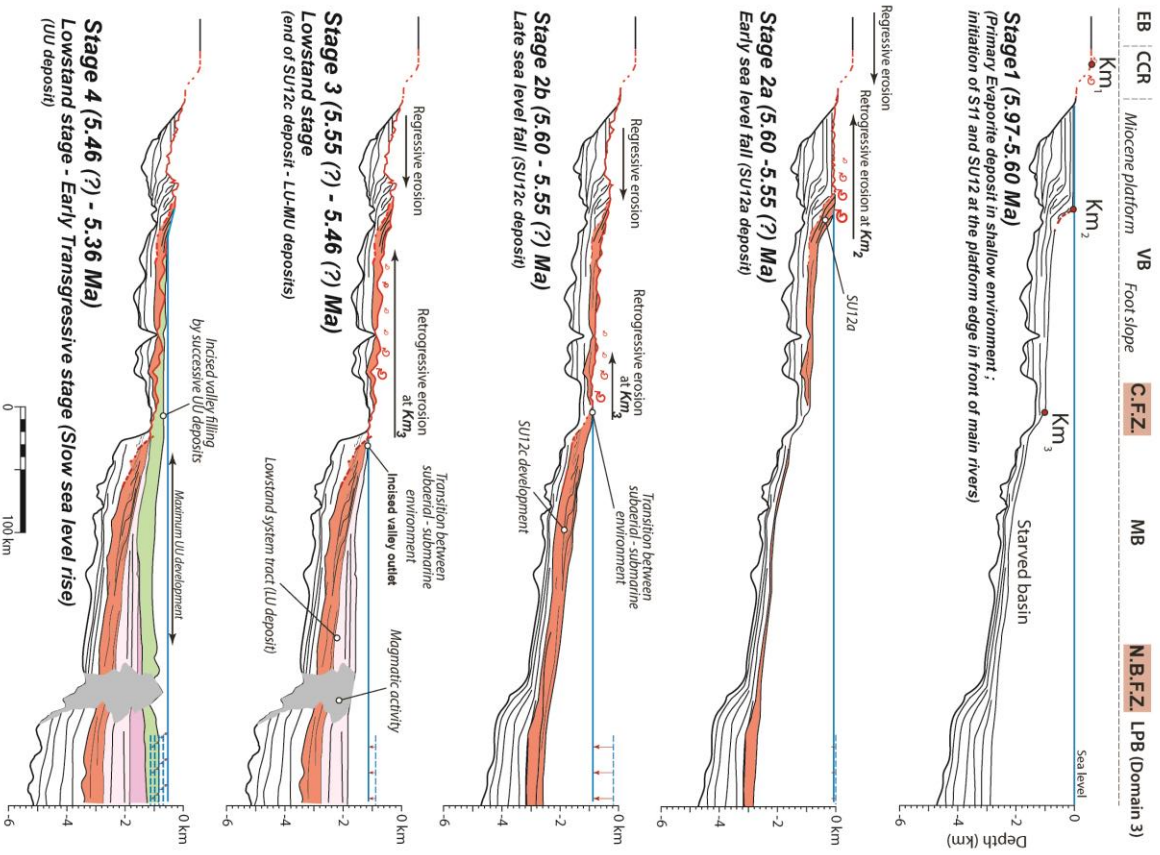


Figure 07

Valencia-Menorca domains



Liguro-Provence domain

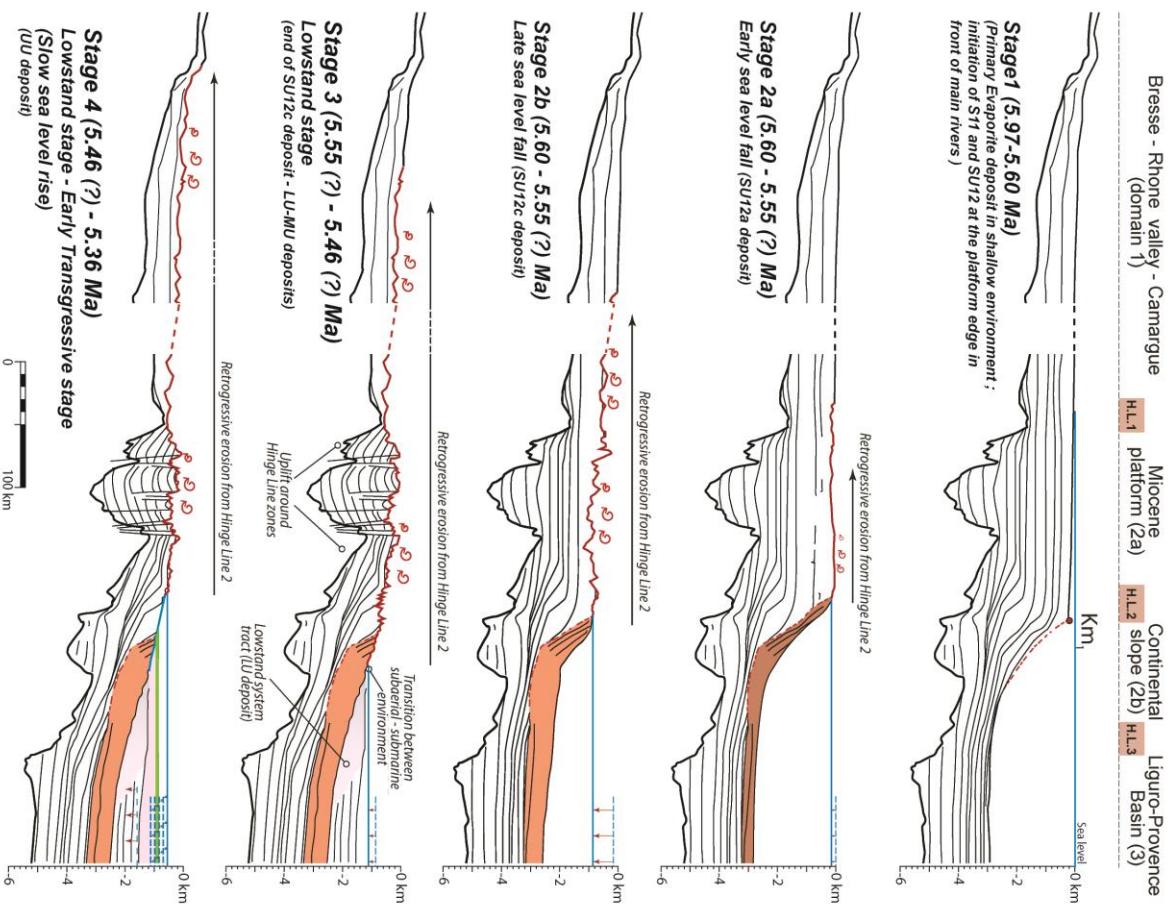
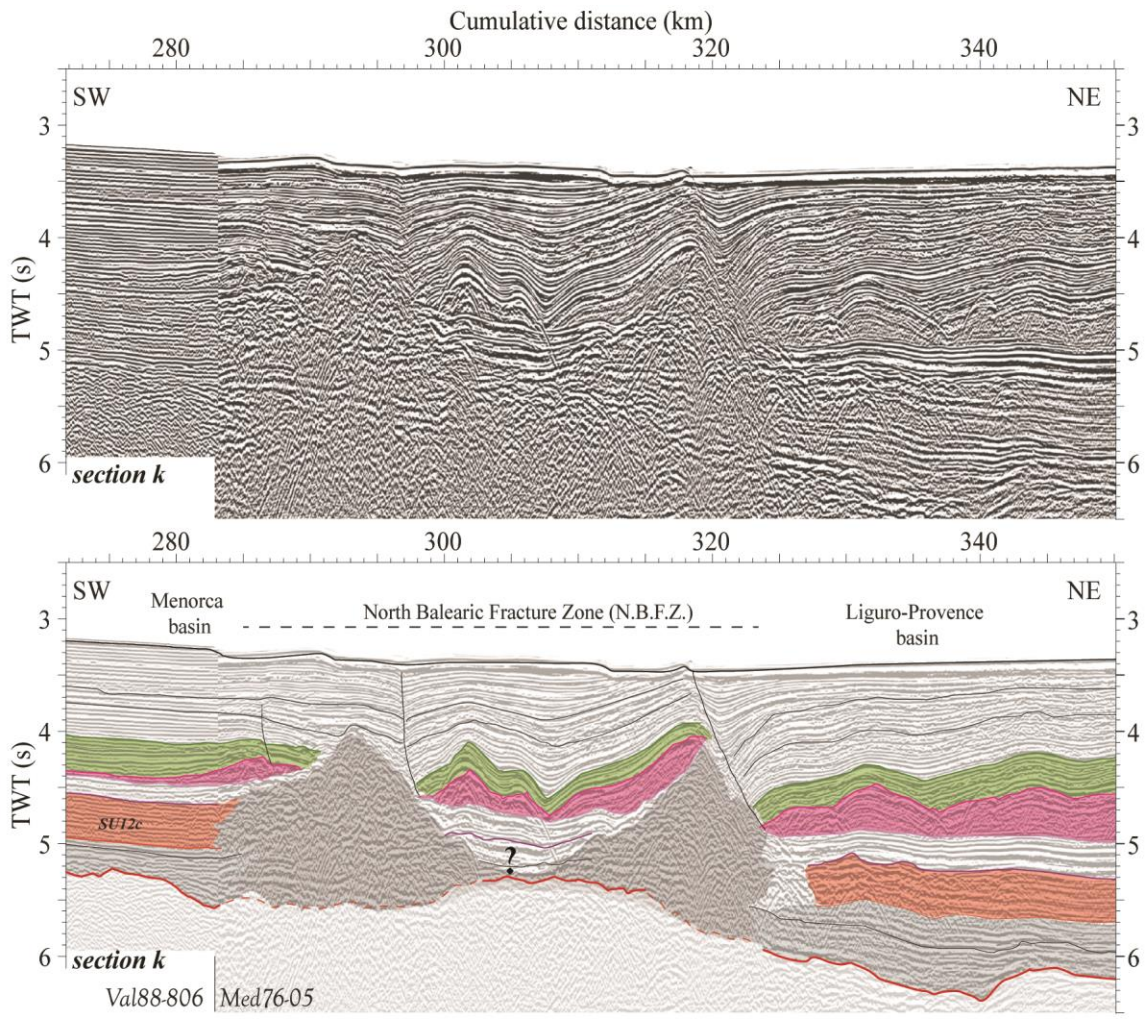


FIGURE 08

831

FIGURE 09

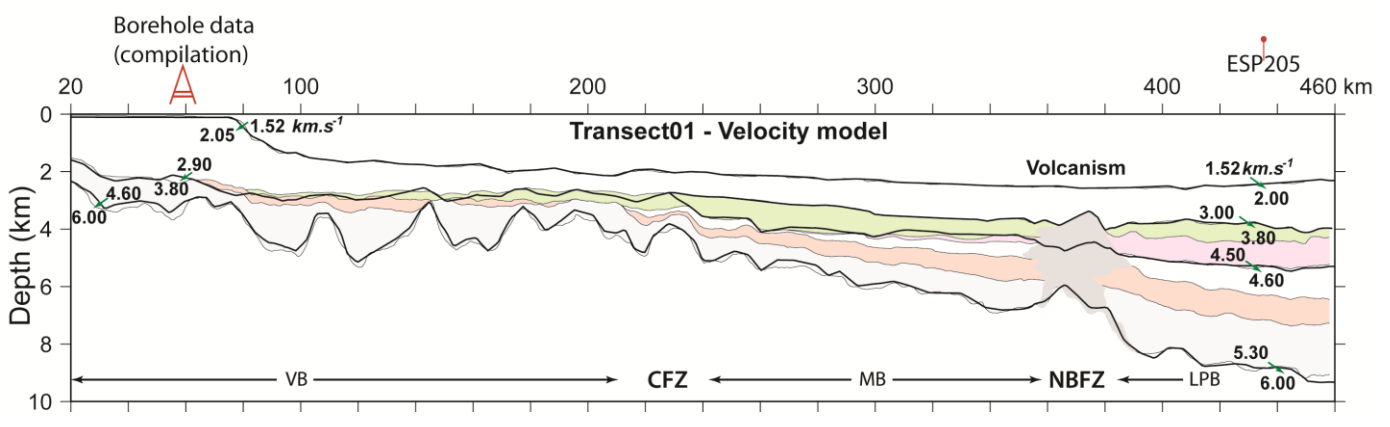


832

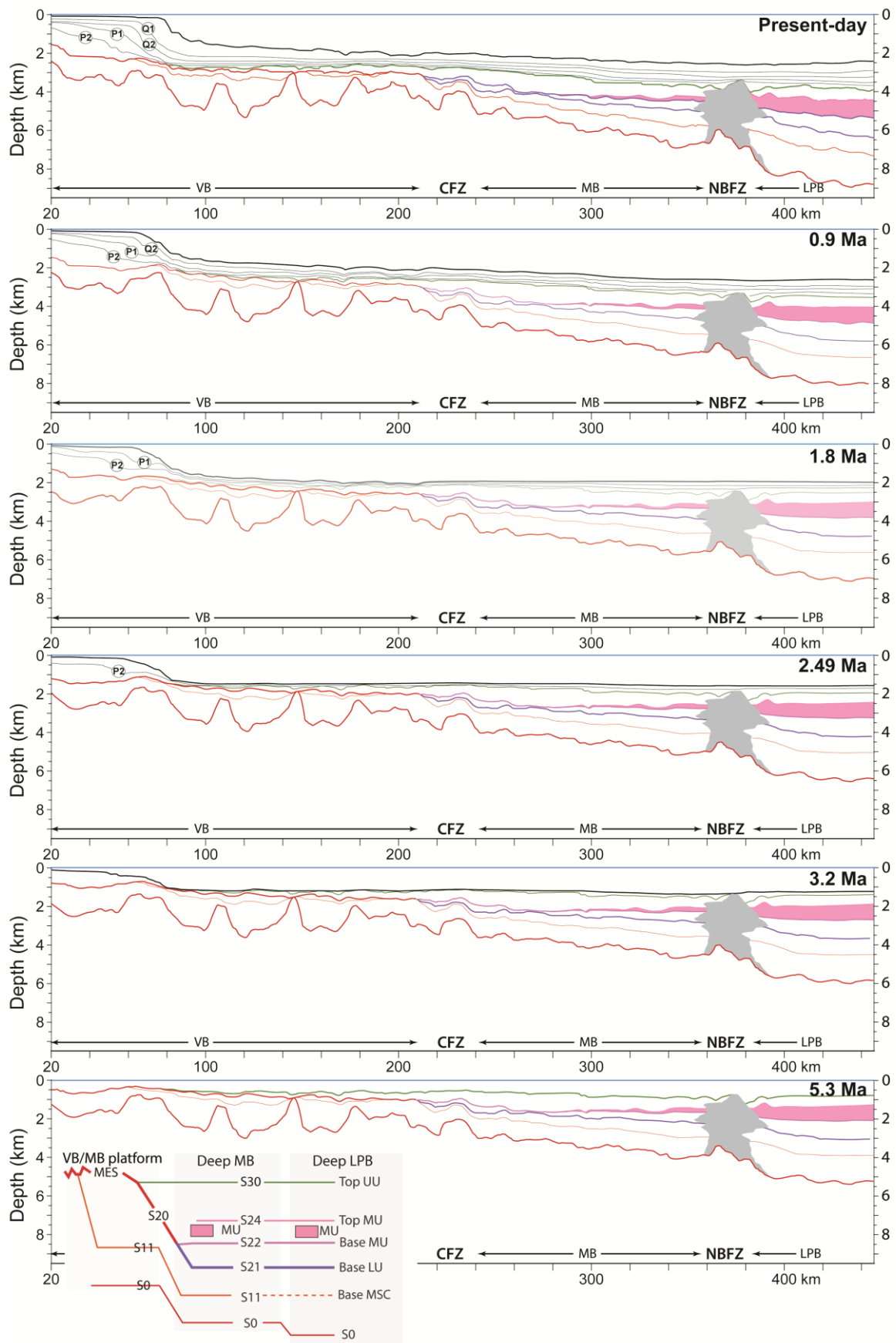
833

834

SUPPLEMENTARY MAT 01



835



Seismic discontinuities	Seismic unit	Seismic facies	Spatial location and observations					Age known/supposed	Interpretations
			VB/MB Platform	VB footslope	MB footslope	MB deep basin	LPB basin (dom. 3)		
Messinian Erosional Surface (MES)		Rough erosive discontinuity	Rough erosive discontinuity until ~1.6 twt	Lateral transition to S20 and S30 at ~ 2.4-2.7 twt				Diachron surface: 5.96-5.32 Ma	Fluvial erosional surface linked to sea level fall
Ravinement Surface (RS) (Hachured blue layer)		Flat discontinuity	- MES/S30 reshaped surface - Conform with SU12 and UU units	—	—	—	—	5.46 (?) - 5.32 Ma	Marine abrasion surface (flattened by the waves)
S30		Erosive discontinuity	—	Upper lateral correlation of MES. Locally conform; high amplitude reflection				5.46 (?) - 5.32 (?) Ma	Marine erosional surface linked to sea level oscillation
	Upper Unit (UU) UUb, c, d	Continuous, sub-parallel reflections of medium-high amplitude	—	UUd development Filling of the incised valley	UUa,b,c,d development with erosional features	UUa, b, c, d max.development Sub-parallel horizons	UU undifferentiated unit Sub-parallel horizons	5.46 (?) - 5.32 Ma	Mixed evaporitic-detrital unit
S26a, b, c		Erosive discontinuity	—	Upper lateral correlation of MES. Locally conform; high amplitude reflection				5.46 (?) - 5.32 Ma	Marine erosional surface linked to sea level oscillation
	UUa	Similar as UUb, c, d	—	—	- At the Top of MU - UUa development conform to MU top unit			5.46 (?) - 5.32 Ma	Mixed evaporitic-detrital unit
S24		Mobile Unit (MU) top surface	—	—	—	Onlap on S21 (Lower Unit top surface)			
	Mobile Unit (MU)	Transparent facies	—	—	—	Full development in LPB Above LU		5.60 (?) - 5.46 (?) Ma	Halite
S22		Conform, continuous high amplitude surface	—	—	—	- MU basal surface -onlap on S21 surface			
	Lower Unit (LU)	Bedded, continuous reflectors of low frequency	—	—	—	- Initiation at Trans-VB outlet at Km3 area - Full development in LPB domain		5.60 (?) - 5.46 (?) Ma	Evaporitic or Mixed evaporitic and detrital
S21		Conform surface ; Lateral evolution of S20	—	—	—	- Slightly erosive at Km3 area - Conform with SU12c and LU			
S20		Erosive discontinuity; margin lateral correlation to MES; Basinward correlation to S21	—	- Erosive surface along trans-VB valley and paleo-relief. - Slightly erosive from either side of the incised valley.		—	—		
	SU12c (Menorca basin)	Prograding clinoform; sub-continuous with moderate amplitude reflectors	—	—	—	- Below LU unit; conformable with LU toward LPB domain; - ONO-ESE prograding trend.		5.97-5.46 (?) Ma	products of messinian erosion
	SU12a (margin)	sub-continuous with moderate amplitude reflectors; cutt and fill geometry	- Below MES and S20 - Above S11; - Bottomset reflectors	- Downstream extension limited by basement high; - Lateral transition with SU12c - SU12a truncated by SU12b		—	—	5.97-5.46 (?) Ma	Earlier marine products of messinian erosion
	SU12b (mass transport deposit) (Maillard et al., 2006)	Chaotic reflectors	—	- Below MES and S20 - Limited by the trans-VB incised valley		—	—	5.97-5.46 (?) Ma	products of messinian erosion/ link to isostatic rebound?
S11		Erosive discontinuity	- Below SU12 units;	- Below SU12 units; - Slightly erosive near paleo-relief; - Conformable surface in the MB / LPB				5.97-5.46 (?) Ma	Basal marine erosive surface
	Primary Evaporite (Del Olmo, 2011) (not show in this study)	Two continuous reflectors with medium-high amplitude	- Below MES and S20 - Only observed along the Sama area	—	—	—	—	5.97-5.60 Ma	Evaporitic deposit in shallow water depth

